https://doi.org/10.5194/egusphere-2024-1086
Preprint. Discussion started: 30 May 2024

A regional analysis of paraglacial landslide activation in southern coastal Alaska

Jane Walden[1,2], Mylène Jacquemart[1,2], Bretwood Higman[3], Romain Hugonnet[1,2,4], Andrea Manconi[5,6], and Daniel Farinotti[1,2]

[1]Laboratory of Hydraulics, Hydrology and Glaciology (VAW), Swiss Federal Institute of Technology (ETH), Zurich, Switzerland
[2]Swiss Federal Institute for Forest, Snow and Landscape Research (WSL), Birmensdorf, Switzerland
[3]Ground Truth Trekking, Seldovia, AK, USA
[4]Department of Civil and Environmental Engineering, University of Washington, Seattle, WA, USA
[5]Institute for Snow and Avalanche Research (SLF), Swiss Federal Institute of Forest, Snow and Landscape Research (WSL), Davos, Switzerland
[6]Department of Earth Sciences, Swiss Federal Institute of Technology (ETH) Zurich, Zurich, Switzerland

Correspondence: Jane Walden (walden@vaw.baug.ethz.ch)

Abstract.

Glaciers worldwide are retreating rapidly due to anthropogenic climate change. One consequence of glacier mass loss is the destabilization of valley walls as the support provided by the glacier changes and eventually vanishes, a process known as "debuttressing." In this work, we examine the evolution of eight large, active instabilities in southern coastal Alaska, a region experiencing some of the fastest glacier retreat worldwide. At half of the sites, the glacier is still in contact with the landslide, while in the other four cases, the terminus retreated past the landslide in recent decades. One site has experienced catastrophic failure; the others have not. We use automatic and manual feature tracking on optical imagery to derive slope movement from the 1980s to present and compare this with glacier terminus retreat and thinning, precipitation, and seismic energy. We find that the majority of sites underwent a pulse of accelerated landslide motion (up to 17 times higher compared to the five years preceding the acceleration) during the studied time period and that the subsequent deformation was independent of the initial activation. In two cases, the acceleration occurred after a particularly rainy month and/or a marked increase (around two times higher than the 1960-2000 average) in glacier thinning. At two further sites, no distinct activation could be detected, though both landslides are known to be moving at velocities below the detection threshold of the methods employed here. In four cases, landslide activation coincided with the rapid retreat (up to 12 times the long term average) of a lake- or marine-terminating glacier past the instability. Our results suggest that landslides adjacent to lake- or marine- terminating glaciers may be especially susceptible to sudden activation, which we hypothesize is due to the faster retreat rates of water-terminating glaciers as well as mechanical and hydrological changes resulting from the replacement of ice with water at the landslide toe. This work shows that glacier retreat can be associated with increasing landslide hazards in various glaciological settings in Alaska, which has implications for the assessment of hazards in a warming world.

https://doi.org/10.5194/egusphere-2024-1086
Preprint. Discussion started: 30 May 2024

1 Introduction

Anthropogenic climate change is causing rapid glacier thinning and retreat all over the world (IPCC, 2022). This glacier mass loss has a wide variety of impacts on the Earth system and human livelihoods, such as sea level rise and changes to glacier runoff (IPCC, 2019; Immerzeel et al., 2020). Glacier retreat may also lead to the destabilization of adjacent valley walls, and this "debuttressing" effect (Ballantyne, 2002) may culminate in the failure of weakened valley slopes. Given that such slopes are often in areas too dynamic to support human infrastructure, there is limited direct risk from landslides. However, they can have significant downstream impacts by damming rivers that might breach as outburst floods, or by erosion of landslide deposits, which can abruptly increase sediment transport (Fan et al., 2020). Additionally, landslides can initiate highly mobile cascading processes which may threaten critical infrastructure (e.g., Van Wyk de Vries et al., 2022; Shugar, D.H. et al., 2021; Sharma et al., 2023).

Where catastrophic landslides enter water, such as proglacial lakes or fjords, they can generate tsunamis. Landslide-tsunami cascades have received attention after several events in deglacierizing regions caused destruction and loss of life. In 1958, for example, a landslide near the terminus of Lituya Glacier, Alaska, impacted Lituya Bay, generating a tsunami that ran up $530\,\mathrm{m}$ on a nearby ridge (Miller, 1960). Less than a decade later, an instability near Grewingk Glacier, Alaska, failed catastrophically into a proglacial lake and caused a tsunami with $60\,\mathrm{m}$ runup (Wiles and Calkin, 1992; Lemaire et al., 2023a). In 2000, a large landslide entered the Vaigat Strait in western Greenland, generating a tsunami with a $28\,\mathrm{m}$ runup in a town $20\,\mathrm{km}$ away from the source (Dahl-Jensen et al., 2004). In 2015, a large landslide in Taan Fiord, Alaska, caused a tsunami with $193\,\mathrm{m}$ runup (Higman et al., 2018). Two years later, in western Greenland, a large landslide failed catastrophically into a fjord, generating a tsunami with $90\,\mathrm{m}$ runup near to the failure site, and the tsunami inundated a village $32\,\mathrm{km}$ away with 1 to $1.5\,\mathrm{m}$ waves (Strzelecki and Jaskólski, 2020). Despite the destructive potential of these events, few cases have been studied in depth, especially in relation to glacier retreat.

There is still much unknown about how glacial erosion and debuttressing may precondition slopes for failure. Higman et al. (2018) identified potential triggering factors at Taan Fiord, such as above-average rainfall and an earthquake, also noting how the glacier retreated over $17\,\mathrm{km}$ in 50 years and thinned by $400\,\mathrm{m}$ from 1961-1991. In the Grewingk case, the exact cause of the failure remains unknown, though it is thought that the slope was weakened by a large earthquake in 1964, a month of intense precipitation, and cycles of glacier retreat (Wiles and Calkin, 1992; Lemaire et al., 2023a). Specifically, upon the formation of the proglacial lake, retreat sped up significantly due to ice loss by calving (Wiles and Calkin, 1992). Here, too, the glacier retreat is thought to have played a role in slope destabilization.

Connections between glacier and landslide changes have been documented at several sites around the world. At the Tungnakvíslarjökull landslide in Iceland, the landslide sped up after the glacier mass loss increased, and glacier debuttressing was determined to be the main cause of slope acceleration (Lacroix et al., 2022). At the Barry Arm landslide in southern Alaska, dramatic landslide acceleration was correlated with rapid glacier retreat (Dai et al., 2020). Interestingly, the kinematic response of the slope to deglaciation has changed throughout time (Schaefer et al., 2023). In a more alpine setting, studies of the Moosfluh landslide in Switzerland showed that glacier unloading and altered groundwater creates critical conditions lead-

https://doi.org/10.5194/egusphere-2024-1086
Preprint. Discussion started: 30 May 2024

ing to enhanced slope instability (Glueer et al., 2020). Numerical models show that thermo- and hydro- mechanical stresses from repeated glacier cycles weaken rock (Grämiger et al., 2018, 2020), and most rock damage occurs upon first deglaciation (Grämiger et al., 2017). Further studies found that the glacier controls the landslide velocity but has little effect on its stability (Storni et al., 2020), and suggested that landslides react rapidly to glacier changes upon crossing a threshold of ice loss (Kos et al., 2016).

These examples indicate that ice loss, whether it be thinning or retreat, is connected to slope instability. They also bring attention to a hazard that is not yet well understood. Alaska, in particular, has come to light as a region where there exists a precarious combination of paraglacial landslide formation and rapidly retreating tidewater or lake-terminating glaciers (Schaefer et al., 2024). This spurred the creation of an Alaskan landslide inventory (Higman, 2022; Higman et al., 2023), which documents instabilities both pre- and post-failure throughout the state. Alaska is also a hotspot for rapid glacier retreat, making up a quarter of global glacier mass loss between 2000 and 2020 (Hugonnet et al., 2021), despite containing only around 12% of the world's glacier volume (Farinotti et al., 2019). Glaciers are projected to continue losing mass at high rates throughout the 21st century (Rounce et al., 2023), which prompts the question of how the risk posed by paraglacial landslides and potential tsunamis will change in the future.

To understand how glacier thinning and retreat control landslide activation and mobility, we take a synoptic view of eight large paraglacial landslides in southern Alaska (Sect. 2) and analyze their evolution using satellite imagery from 1984 until present, surface velocity changes from 1984-2022, and elevation changes from the mid-1900s until 2020. By doing so, we provide the first detailed regional study examining the impact of glaciers on slope stability in Alaska. Specifically, we ask whether the (re-)activation of paraglacial landslides can be explained by glacier retreat. In order to evaluate the relevance of the glacier changes, we also consider meteorological and seismic influences (Sect. 3). We combine these data to assess whether and how glacier changes can be responsible for slope destabilization (Sect. 4) and discuss these in the context of the possible physical mechanisms behind the slope instabilities (Sect. 5).

2 Study Area

Southern Alaska is heavily glaciated, hosting some of the largest glaciers in the world (Windnagel et al., 2023). It has a maritime climate due to its proximity to the ocean, leading to high annual precipitation and in turn, extensive glacier coverage (Shulski and Wendler, 2007). Over the eight study sites (Fig. 1) and the period 1979-2022, annual precipitation ranges from 2670 to $4030\,\mathrm{mm}$ while mean annual air temperatures are between -4 and $1\,^{\circ}\mathrm{C}$ (Hersbach et al., 2018). These large precipitation amounts result in a thick winter snowpack which, combined with relatively mild temperatures, make extended permafrost coverage unlikely (Figure 1; Obu et al., 2018).

Glacier mass loss since the Little Ice Age in Alaska is resulting in high isostatic rebound rates. This, in combination with the Alaska's location on a subduction zone, causes some of the world's highest uplift rates: up to $32\,\mathrm{mm\,yr^{-1}}$ in southeastern Alaska. In this area, up to $5\,\mathrm{mm\,yr^{-1}}$ of the total uplift is due tectonic forcing, 2 to $4\,\mathrm{mm\,yr^{-1}}$ comes from global glacier isostatic adjustment, as much as $13\,\mathrm{mm\,yr^{-1}}$ are due to current glacier mass loss, and the rest (ca. $10\,\mathrm{mm\,yr^{-1}}$) are due to

https://doi.org/10.5194/egusphere-2024-1086
Preprint. Discussion started: 30 May 2024

viscoelastic uplift (Larsen et al., 2005). The collision of the Pacific and North American plates has formed several major faults throughout the state. The Castle Mountain, Border Ranges, and Fairweather faults are the most relevant for this work (Mériaux et al., 2009). Alaska is one of the most seismically active regions in the world, having had four of the twenty largest earthquakes recorded globally since 1900 (Earthquake Hazards Program, 2019), and with an earthquake of magnitude eight or larger every 13 years since 1900 (Alaska Seismic Hazards Safety Commission, 2012). The state also sees many moderate earthquakes of magnitude 4 to 5: on average, 300 per year since 1900 (Alaska Seismic Hazards Safety Commission, 2012).

Study sites were selected from the *Alaska inventory of landslides and slope instabilities* (Higman, 2022; Higman et al., 2023). In line with the terminology used in the inventory, we use the terms "landslide" and "instability" interchangeably throughout this publication. The inventory contains over 780 landslides at the time of publication, and details the instability characteristics, location, date of slope failure (if available), volume, and the hazard potential to communities and infrastructure. From the complete inventory, we selected a subset of eight sites in southern coastal Alaska that met the following criteria:

1. Volume estimated to be greater than $10\,\mathrm{Mio.\,m^3}$,
2. In contact with a glacier at some stage since the 1980s,
3. Geomorphic signs of recent movement after the mid-1980s.

If there were several sites in a close proximity that matched these criteria, the largest and most active instability was selected. The selected sites are shown in Figure 1 and Figure 2, and are described further in the following subsections.

2.1 Ellsworth

Ellsworth Glacier is a lake-terminating glacier located on the Kenai Peninsula, around $30\,\mathrm{km}$ east of Seward, Alaska (Fig. 1B and Fig. 2). It is oriented to the southwest and flows from a glacier complex at over $1800\,\mathrm{m\,a.s.l.}$ to nearly sea level ($10\,\mathrm{m\,a.s.l.}$). There are a series of instabilities along the western edge of the glacier, where the glacier bends. We focus on the instability which is largest and farthest up-glacier, spanning a distance between 2.5 and $4\,\mathrm{km}$ from the 2021 terminus. The instability is characterized by a prominent main scarp and an active talus source area (Higman et al., 2023). Movement at the site between 2016 and 2022 has been confirmed by Schaefer et al. (2024) using interferometric synthetic aperture radar (InSAR). The instability is located in sedimentary rocks of the Orca group (Eocene to Paleocene age) and the lithology of the group is sedimentary, consisting primarily of sandstone and siltstone (Wilson et al., 2015). The volume is estimated between 66 and $150\,\mathrm{Mio.\,m^3}$ (14 to $113\,\mathrm{Mio.\,m^3}$ according to Schaefer et al. (2024); Tab. C2 and App. C).

2.2 Portage

Portage Glacier is a lake-terminating glacier located at the northern part of the Kenai Peninsula, around $7.5\,\mathrm{km}$ southwest of Whittier, Alaska (Fig. 1A and Fig. 2). The glacier flows northeast and extends from an ice field at $1430\,\mathrm{m\,a.s.l.}$ to around $60\,\mathrm{m\,a.s.l.}$. At the north end of the glacier, where the glacier calves into Portage Lake, there are two instabilities. We focus on the larger and more active of the two, laying farther up-glacier, between 200 and $1100\,\mathrm{m}$ from the 2021 terminus. The

https://doi.org/10.5194/egusphere-2024-1086
Preprint. Discussion started: 30 May 2024

instability shows clear signs of deformation including tension cracks, a main scarp, a talus source area, and antiscarps (Higman et al., 2023). Rockfall activity has been observed at the site and surficial streams on the slide disappear into the subsurface (Higman et al., 2023). InSAR data suggest the landslide moved between 2016 and 2022 (Schaefer et al., 2024). The instability is located in Chugach flysch (Upper Cretaceous age) and the lithology is sedimentary, composed primarily of metagraywacke and metasiltstone (Wilson et al., 2015). The instability has a volume of around 11 to 35 Mio. m^3 (5 to 19 Mio. m^3 according to Schaefer et al. (2024); Tab. C2 and App. C).

2.3 Barry

Barry Glacier is a tidewater glacier flowing southwest into Barry Arm in Prince William Sound, around $50\,\mathrm{km}$ northeast of Whittier, Alaska (Fig. 1A and Fig. 2). The glacier flows from an accumulation area in a large ice complex in the Chugach Mountains at $2700\,\mathrm{m\,a.s.l.}$ to sea level. The region around the glacier terminus is very dynamic. There are a number of instabilities to the northwest and southeast of the terminus. We focus on the largest instability, which is characterized by anti- and normal-scarps, a main scarp, and a talus slope area (Higman et al., 2023). Multiple studies have confirmed the movement of this landslide since 2000 (Dai et al., 2020; Schaefer et al., 2024). Like Portage, the Barry instability is located in Chugach flysch. As of 2021, around half of the landslide toe was buttressed by the glacier, though the glacier has been retreating past the instability since 2010. The Barry instability is the second largest in this study, with an estimated volume of 188 to 500 Mio. m^3 (117 to 564 Mio. m^3 according to Schaefer et al. (2024); Tab. C2 and App. C).

2.4 Yale

Yale Glacier is a tidewater glacier terminating in College Fiord in Prince William Sound, approximately $70\,\mathrm{km}$ northwest of Valdez, Alaska (Fig. 1A and Fig. 2). It flows from a large glacier complex in the Chugach Mountains at around $3600\,\mathrm{m\,a.s.l.}$ to sea level. Within $2\,\mathrm{km}$ of the present-day terminus, there are three instabilities. We focus on the largest of the three, which has a volume between 255 and 750 Mio. m^3 (145 to 1025 Mio. m^3 according to Schaefer et al. (2024); Tab. C2 and App. C). The instability is characterized by anti- and normal-scarps, a talus slope area, shear zones, and tension cracks (Higman et al., 2023), and movement of the landslide has been confirmed with InSAR (Schaefer et al., 2024). As with the other nearby instabilities, the lithology of this site is Chugach flysch. Debuttressing of the landslide began around 1977, but it took until 2021 for the terminus to completely retreat past the toe area.

2.5 Columbia

Columbia Glacier, located around $35\,\mathrm{km}$ northwest of Valdez, Alaska (Fig. 1A and Fig. 2), is likely one of the most well-known glaciers worldwide due to its striking retreat over the past decades. The highest reaches of the glacier are nearly $3700\,\mathrm{m\,a.s.l.}$ in the Chugach Mountains and it flows to the south down to sea level in Prince William Sound. Near the present-day terminus of Columbia Glacier, there are several instabilities to the north. We select the instability which is closest to the terminus (between 500 and $1800\,\mathrm{m}$ in 2021) and which could pose the largest hazard in the coming decades. The instability is characterized by

https://doi.org/10.5194/egusphere-2024-1086
Preprint. Discussion started: 30 May 2024

tension cracks, normal scarps, a talus slope, and a lake which drains periodically (Higman et al., 2023). InSAR results from Schaefer et al. (2024) suggest the landslide moved between 2016-2022. The lithology of the instability is Chugach flysch. It has a volume of approximately 44 to 150 Mio. m^3 (17 to 111 Mio. m^3 according to Schaefer et al. (2024); Tab. C2 and App. C).

2.6 Tyndall

Tyndall Glacier is located in the St. Elias mountain range and terminates at sea level in Taan Fiord, around 110 km northwest of Cordova, Alaska (Fig. 1C and Fig. 2). The glacier is bordered by some of Alaska's tallest mountains, with an accumulation area reaching up to 5290 m a.s.l.. There are a number of instabilities near the terminus of Tyndall Glacier. We select the one that failed catastrophically in 2015, which had a volume of 63 Mio. m^3 and caused a tsunami with 193 m runup (Higman et al., 2018). The remaining sliding mass is around 100 Mio. m^3 (Tab. C2 and App. C). This site is thus distinct from the others because it has already experienced a catastrophic failure. The instability at Tyndall is located in the Kulthieth Formation, a sedimentary lithology from the Eocene composed of conglomerate-mudstone (Wilson et al., 2015). As of 2021, the glacier buttresses the length of the landslide toe. After a rapid retreat in the late 1980s, the glacier terminus was up-valley with respect to the landslide but has been stable or slowly advancing since the early 1990s.

2.7 Alsek

Alsek Glacier is located in southeastern Alaska, around 100 km from Yakutat (Fig. 1D and Fig. 2). Alsek Glacier flows from an elevation of 2420 m a.s.l. down to 60 m a.s.l.. The glacier terminates in Alsek Lake, which has grown from a few square kilometers in the 1950s to about 75 km^2 today as the glacier has retreated (Loso et al., 2021). Between 3.5 and 5 km up-glacier from the 2021 terminus, an instability with a volume between 19 and 50 Mio. m^3 (Tab. C2 and App. C) is found on the eastern side of a nunatak. The failure is characterized by a large head scarp which extends around 1 km laterally. The instability at Alsek Glacier is found in volcanic rocks of the Chugach accretionary complex, a metamorphic lithology from the Upper Cretaceous (Wilson et al., 2015). Gneiss, migmatite, and schist are the primary rock types (Wilson et al., 2015).

2.8 Grand Plateau

Grand Plateau Glacier is located in southeast Alaska, around 120 km from Yakutat (Fig. 1D and Fig. 2). It is a very large glacier, spreading over an area of 237 km^2 and spanning an elevation range of nearly 4600 m. The glacier currently terminates in three different lakes. We focus on the southeastern branch, where an instability with a volume of 50 to 150 Mio. m^3 is present (Tab. C2 and App. C). The instability at Grand Plateau Glacier is located on an east-facing mountainside at the glacier left. The terminus began retreating past the instability around 2010, and the instability was completely debuttressed in 2022. It displays signs of movement through scarps, and like Alsek, it is located in volcanic rocks of Chugach accretionary complex.

https://doi.org/10.5194/egusphere-2024-1086
Preprint. Discussion started: 30 May 2024

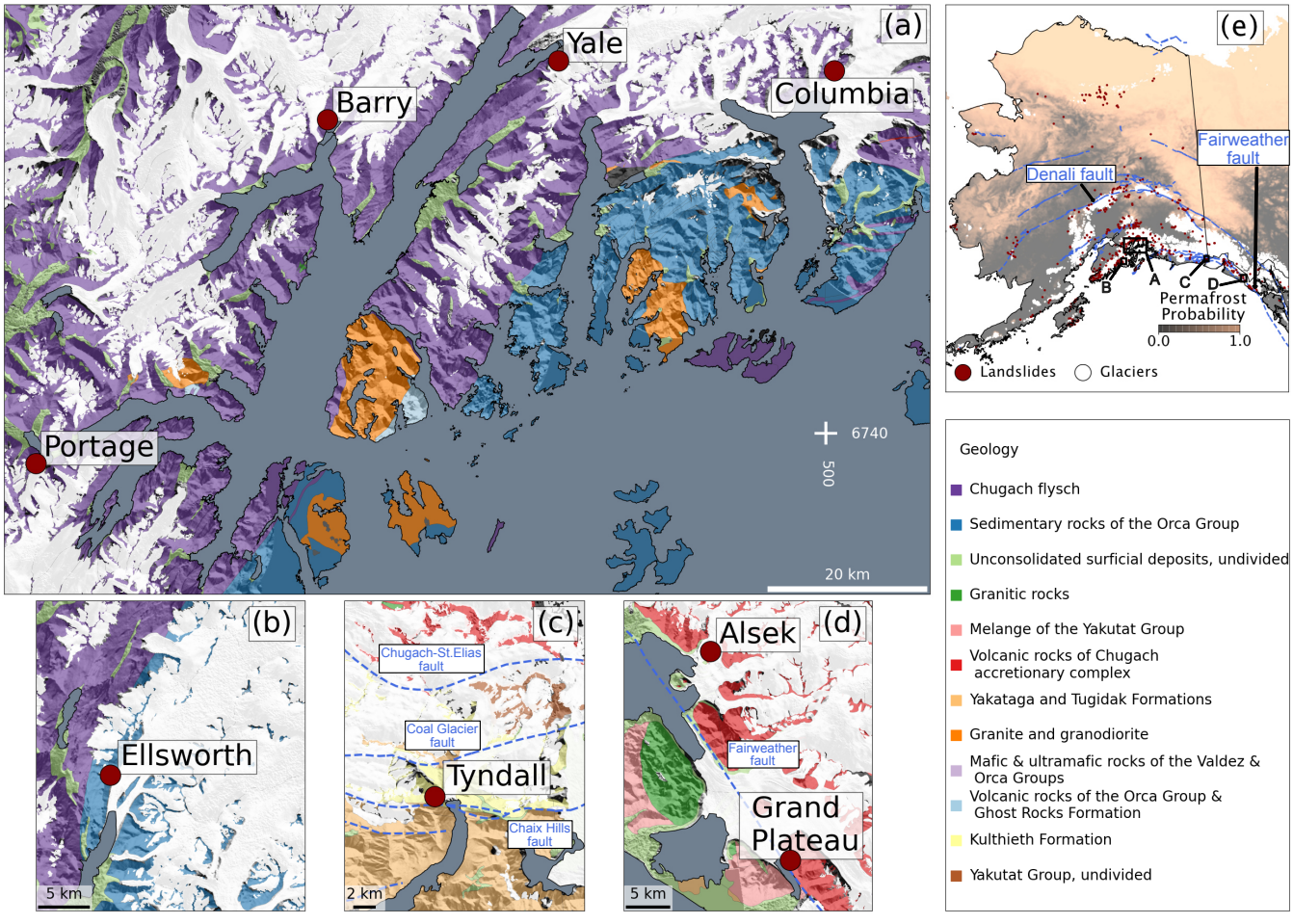

Figure 1. Overview of the sites of interest. Panels A-D (see panel E for location within Alaska) show the geology of the region (Wilson et al., 2015), with the legend at bottom right. Sites of interest are labeled with dark red points. Ocean area (gray) is from © OpenStreetMap contributors 2024. Distributed under the Open Data Commons Open Database License (ODbL) v1.0. A 2000s digital elevation model is used as a background layer (Hugonnet et al., 2021). Panel E shows the permafrost probability (Obu et al., 2018), along with all sites from Higman (2022) (red dots), the glacierized area from RGI Consortium (2017) (white area), and faults from U.S. Geological Survey and Alaska Department of Natural Resources (2024) (blue dashed lines).

https://doi.org/10.5194/egusphere-2024-1086
Preprint. Discussion started: 30 May 2024

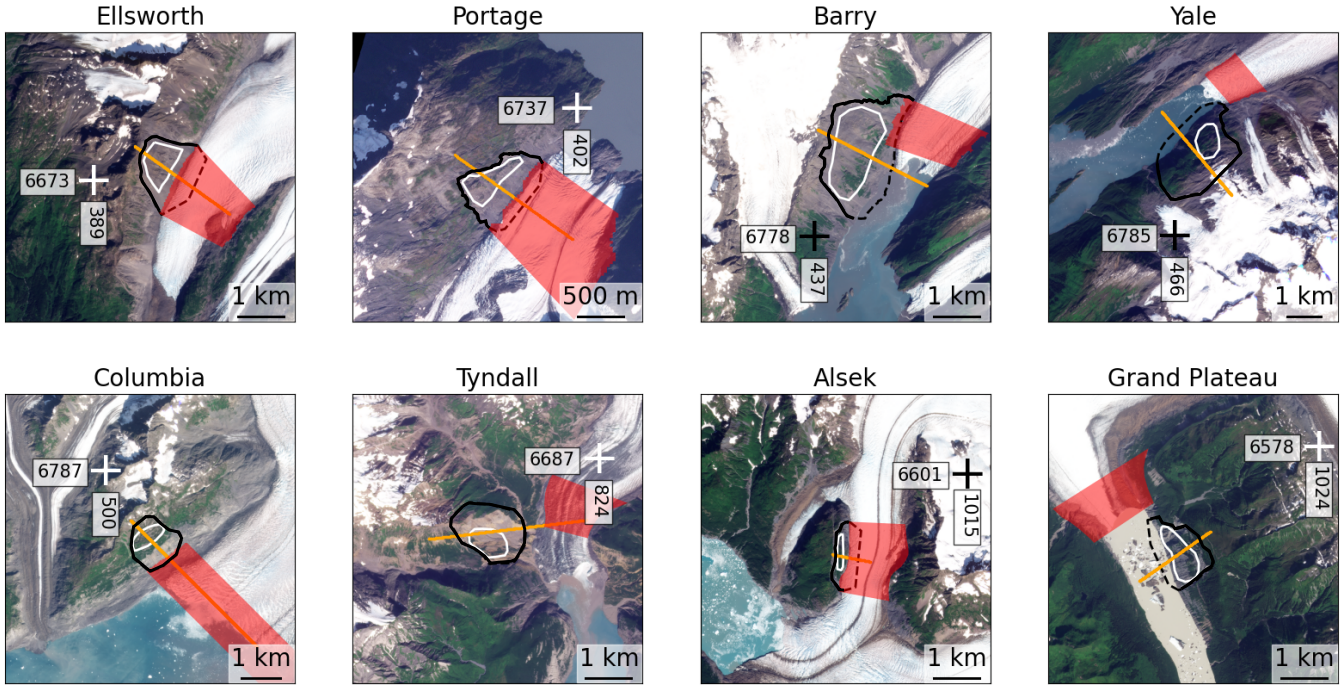

Figure 2. Satellite imagery from August 2023 over the eight investigated sites (see Fig. 1 for location). Instability outlines are shown in black, and dashed lines provide an estimate for the instability extents that are not visible at the surface (subglacial or submarine extents). In the text, the resulting area is referred to as "instability polygon" (see App. C for a description). The "active area" (described in Sect. 3.1) is shown in white, and the cross section (described in Sect. 3.2 and App. E) is plotted in orange. The "IAG polygon" (see Sect. 3.2 and App. E) is plotted in red. Coordinates crosses refer to the UTM 6 projected coordinate system. The source of all images is Planet Labs PBC.

3 Data & Methods

In order to understand how glacier thinning and retreat control the mobility of the investigated landslides, we analyzed their deformation in response to glacier and environmental changes over the past 40 years. Specifically, we characterized their deformation from a combination of automatic and manual feature tracking on satellite optical imagery, and combined this with several parameters describing glacier change. We determined glacier retreat rates by mapping yearly terminus positions and quantified glacier thinning rates from digital elevation model (DEM) differencing. From these data we evaluated whether any acceleration of the paraglacial landslide coincided with changes in glacier behavior. Finally, to gauge the importance of the glacier-related controls, we evaluated time series of precipitation and seismicity as possible alternative drivers of landslide mobility. The details of the individual datasets and methods applied are presented in the following sections.

https://doi.org/10.5194/egusphere-2024-1086
Preprint. Discussion started: 30 May 2024

3.1 Landslide displacements

We retrieved landslide velocities from the ITS-LIVE annual mosaics (Gardner et al., 2023). The dataset was originally developed to map glacier flow, but it extends beyond the glacier boundaries and allows for applications on neighboring slopes. ITS-LIVE data is generated from Landsat 4-8 image pairs and processed using the autonomous Repeat Image Feature Tracking algorithm (auto-RIFT; (Gardner et al., 2018)). For each year between 1984 and 2022, the following relevant parameters are available: velocity magnitude, velocity components in the x- and y- directions, and an estimate for the uncertainty in the velocity. The resolution of the product is 120 m. While the resolution is not enough to distinguish accelerations of small scale features, it is sufficient to determine velocity changes at the scale of the landslides we consider.

For each year in the ITS-LIVE dataset we extracted the velocity and uncertainty over the ”active area" of the instability (see below). The median velocity and uncertainty were computed over this area, thus creating an annual time series. The active area was delineated by selecting velocity pixels which fell within the instability polygon (see Fig. 2 for definition) and which showed movement in the 1984-2022 ITS-LIVE velocity magnitude data (Fig. 3). We excluded glacier pixels as defined by the RGI Consortium (2017), as well as any pixels adjacent to the glacier which had a high velocity compared to the instability and moved parallel to the glacier. At sites where no motion was detected by ITS-LIVE, we selected pixels over the area where most deformation is seen from satellite images.

We supplement the data from ITS-LIVE with measurements from manual feature tracking on the Landsat data at approximately five year time steps. We do this for two reasons: i) pre-2000 ITS-LIVE data has relatively high uncertainty and we question its reliability and ii) visual inspection of the Landsat images over longer time steps (5 to 10 years) often show clearly visible changes that are not picked up by automatic feature tracking. We therefore selected cloud- and snow-free summer images on average every 5 to 6 years (some images were as little as 3 years or as much as 12 years apart) and manually mapped displacements indicating coherent motion throughout the slope. We classified movement as “coherent” or “slope-wide” if large vegetated patches within the instability polygon synchronously moved in a given direction. Displacement or alteration of isolated vegetation patches did not classify as movement in the analysis. For slopes that experienced catastrophic failure, no feature tracking was done after the failure because the fundamental changes of the sliding mass make the pre- and post-failure slopes incomparable. The velocity was computed by determining the average distance travelled by individual features over the time period covered by two consecutive images, and by then dividing that distance by the corresponding number of years.

3.2 Surface elevation changes

To quantify glacier thinning or thickening, as well as landslide subsidence or thickening, we computed the differences between seven different DEMs: a 1960s DEM from Berthier et al. (2010), a 1978 DEM from Dehecq et al. (2020), and the 2000, 2005, 2010, 2015, and 2020 DEMs from Hugonnet et al. (2021). Both the 1960s and 1978 DEMs are composites from different years. The DEM by Berthier et al. (2010) was generated from historical USGS maps produced between 1948 and 1972, although for the glaciers of interest the information stems primarily from a single year (small portions in the accumulation area might stem from another year). The DEM has a spatial resolution of 40 m and for simplicity we will refer to it as the 1960s DEM. The

https://doi.org/10.5194/egusphere-2024-1086
Preprint. Discussion started: 30 May 2024

DEM from Dehecq et al. (2020) is generated from declassified analog satellite stereo-images from the American reconnaissance program Hexagon (KeyHole-9) and covers the late 1970s. Here, the dates range from 1977 to 1980, but we will refer to this as the 1978 DEM. This DEM has a spatial resolution of 48 m. The DEMs from Hugonnet et al. (2021) cover the 21st-century and have a spatial resolution of 30 m. These DEMs were created by temporal interpolation of several repeat DEMs either generated from stereo-images from the Advanced Spaceborne Thermal Emission and Reflection Radiometer (ASTER) or retrieved from the ArcticDEM strip archive based on WorldView stereo-images (Porter et al., 2018). At each pixel, on average 40 independent ASTER or ArcticDEM elevations acquired in the period 2000–2019 are used to predict elevation at the specific dates of 2000, 2005, 2010, 2015 or 2020.

Prior to extracting the elevation changes from the DEMs, we co-registered them all to the 2000 DEM to correct for shift and tilt misalignments. Horizontal and vertical shifts were removed following the iterative slope–aspect method of Nuth and Kääb (2011), then tilts were removed by fitting a 2-dimensional plane to elevation change residuals. Finally, we repeated the horizontal and vertical shift coregistration to remove sub-pixel shifts introduced by the tilt correction. This coregistration pipeline was performed using the *xdem* package (xdem contributors, 2021). The terrain used for coregistration was restricted to areas within $20\,\mathrm{km}$ of the glaciers of interest but excluding areas within $2\,\mathrm{km}$ of their RGI Consortium (2017) outlines. There was a shift of $2\,\mathrm{m}$ on average, consistent with the offset reported by Berthier et al. (2010). The vertical reference of the 1960s DEM had to be transformed from the EGM96 geoid to the WGS84 ellipsoid. The vertical shifts resulting from the transformation were between -10 and $20\,\mathrm{m}$, depending on the location in Alaska.

We computed surface elevation changes over the following time periods: 1960–1978, 1978–2000, 2000–2005, 2005–2010, 2010–2015, 2015–2020. Note that no elevation data is available for Ellsworth and Columbia in 1978 so the changes over 1960–2000 were computed. We then examined the spatial distribution of the elevation changes throughout time, particularly over the glacierized area next to the landslide, and searched for periods of rapid thinning. The interpretation was aided by defining both a cross section and an instability-adjacent glacier (IAG) polygon (see Fig. 2 and Sect. E for descriptions). Using the cross section, we extracted values from the seven DEMs to create elevation profiles. Using the IAG polygon, we computed the median elevation change over the glacierized area near the instability in different time periods.

3.3 Glacier terminus position

We used time series of glacier terminus positions mapped from Landsat images (1985–2022) to quantify glacier retreat and occasional glacier advance at yearly time steps. For Barry, Yale and Columbia, these data were already available until 2012 from McNabb et al. (2015), which provides manually-digitized terminus positions using all available Landsat images. For the other sites (Ellsworth, Portage, Tyndall, Alsek, and Grand Plateau), we manually mapped the terminus positions on an annual basis using cloud-free summer images to minimize snow cover. A list of images used for delineation is found in the Supplementary Materials.

Glacier retreat rates were then calculated along the central flow lines of the glaciers. These centerlines were taken from RGI v6 (RGI Consortium, 2017), though we had to manually extend them down valley to account for the larger glacier extents during the early years of our study period (RGI outlines represent the glacier states around the year 2000). In some cases

https://doi.org/10.5194/egusphere-2024-1086
Preprint. Discussion started: 30 May 2024

we manually refined the automatically generated RGI centerlines to more accurately represent the glacier and valley shapes. Finally, we calculated the retreat by intersecting the centerlines with the glacier terminus positions, and cumulating the retreat relative to the largest glacier extent.

3.4 Supporting glacier and environmental data

3.4.1 Ice thickness

We used the two global ice thickness datasets by Farinotti et al. (2019) and Millan et al. (2022) to determine the valley topography below the glacier, put ice thinning rates into context, and estimate the ice remaining in front of the landslides. Two ice thickness products were used in order to increase the robustness of the result and to obtain a range of possible values. Both Farinotti et al. (2019) and Millan et al. (2022) determine ice thickness using surface characteristics, such as elevation, slope, and ice velocity. Farinotti et al. (2019) ice thickness dates refer to the glacier outlines from RGI Consortium (2017), while Millan et al. (2022) corresponds to the year 2017-2018.

The elevation of the glacier bed was determined by subtracting the given ice thicknesses from a 2015 DEM (Hugonnet et al., 2021). Note the usage of a DEM that does not correspond to the year of the ice thickness introduces some error, but we expect this to be minor in comparison to the ice thickness uncertainty. Using the defined cross sections (Sect. E), we extracted the bedrock elevation resulting from each thickness dataset. Similarly, we computed the median thickness within the IAG polygon (see Sect. E) from both datasets.

3.4.2 Meteorology

We extracted time series of monthly temperature and precipitation from ERA5 reanalysis data (Hersbach et al., 2018) to determine if meteorological changes may correlate with landslide activity. For each site, we selected the grid cell (0.25° x 0.25°) encompassing the instability and retrieved the monthly values from 1979 until 2022. We averaged monthly temperature values and summed monthly precipitation values to get annual values.

We inspected the data for changes in meteorological conditions which may explain increased slope activity, such as particularly rainy months or years. To do so, we determined the average and standard deviation of the monthly precipitation. We then investigated if periods of increased slope activity corresponded to times with particularly high precipitation (exceeding two standard deviations above the mean). In addition to the monthly analysis, we used the *pymannkendall* package (Hussain and Mahmud, 2019) to determine long-term trends in the yearly time series.

3.4.3 Seismology

We used the USGS Earthquake Catalog to extract all seismic events in the study area between 1980 and 2023 (U.S. Geological Survey, 2023). We selected earthquakes which were within $100\,\mathrm{km}$ of a study site and that had a magnitude $\geq$4. Magnitude 4 is widely considered to be the threshold at which earthquakes can cause landslides (Keefer, 1984). However, we acknowledge

https://doi.org/10.5194/egusphere-2024-1086
Preprint. Discussion started: 30 May 2024

that pre-1980s events, as well as repeated smaller earthquakes, may have caused rock damage that permanently destabilized the slope.

We are interested in quantifying the effect of seismic activity on slope stability, since seismic activity may induce rock mass fatigue and promote failure (Gischig et al., 2016). Using the above dataset, we estimate an intensity of the seismic events at the location of the investigated instabilities. To do so, we first calculate the energy E released by each earthquake. For an earthquake with magnitude M, this is given by $E = 10^{(5.24+1.44*M)}$ (Earthquake Hazards Program, 2024). We then estimate a location-specific intensity I, which we define as the quotient of the earthquake energy E and the square of the distance d between the instability and the earthquake epicenter:

$$I(t) = \sum_{t} \frac{E(t)}{d^2}. \tag{1}$$

Here, t is the time since 1980, and the summation is meant to represent the cumulative energy experienced at each site up to the given point in time. We inspected the resulting time series for periods where the cumulative seismic intensity increased sharply, and assessed whether such periods coincided with increased slope activity.

4 Results

To understand how glacier retreat controls landslide activity, we analyzed landslide displacements and glacier behavior from the early 1980s to present-day. In the following, we first describe the most important stages of the landslide evolution at each site, and then describe the glacier activity during these stages. We summarize the temporal connections between the landslide and glacier changes, and present the findings of both the meteorological and seismic investigations.

4.1 Landslide evolution

Seven out of eight sites displayed clear down-slope movement between 1984 and 2022 (Fig. 3), moving at average speeds of $\sim$3.4 to $\sim$8.6 $\mathrm{m\,yr^{-1}}$. At six of these sites, the combined use of ITS-LIVE data and manual feature tracking revealed distinct periods of acceleration or large surface changes (Fig. 4). During these times, the landslide velocities from ITS-LIVE increased by a factor of two (Grand Plateau) to seventeen (Ellsworth) compared to the average velocity in the five years prior to the acceleration. In the following, we will discuss the behavior of individual landslides in more detail.

At Tyndall and Yale, landslide activity began as early as the 1980s and 1990s, respectively. At Tyndall, a 60 m-wide crack opened at the top of the landslide between 1987 and 1990 (Fig. 4c1 and Fig. 6C). Further disintegration of the slope followed, including slope-scale motion starting in the 2000s, culminating in the catastrophic failure of 2015. While around 60 Mio. $\mathrm{m^3}$ fell into the fjord, another 100 Mio. $\mathrm{m^3}$ remain on the slope and have continued moving slightly since 2015. At Yale, manual feature tracking between 1989-1995 shows that the landslide experienced a sudden pulse of movement (Fig. 4b1 and Fig. 6B), with surface features being displaced by around 75 m. The location of these surface displacements coincides with the area of increased activity visible in the ITS-LIVE data (Fig. 3). Based on manual feature tracking, we did not detect any visible motion

https://doi.org/10.5194/egusphere-2024-1086
Preprint. Discussion started: 30 May 2024

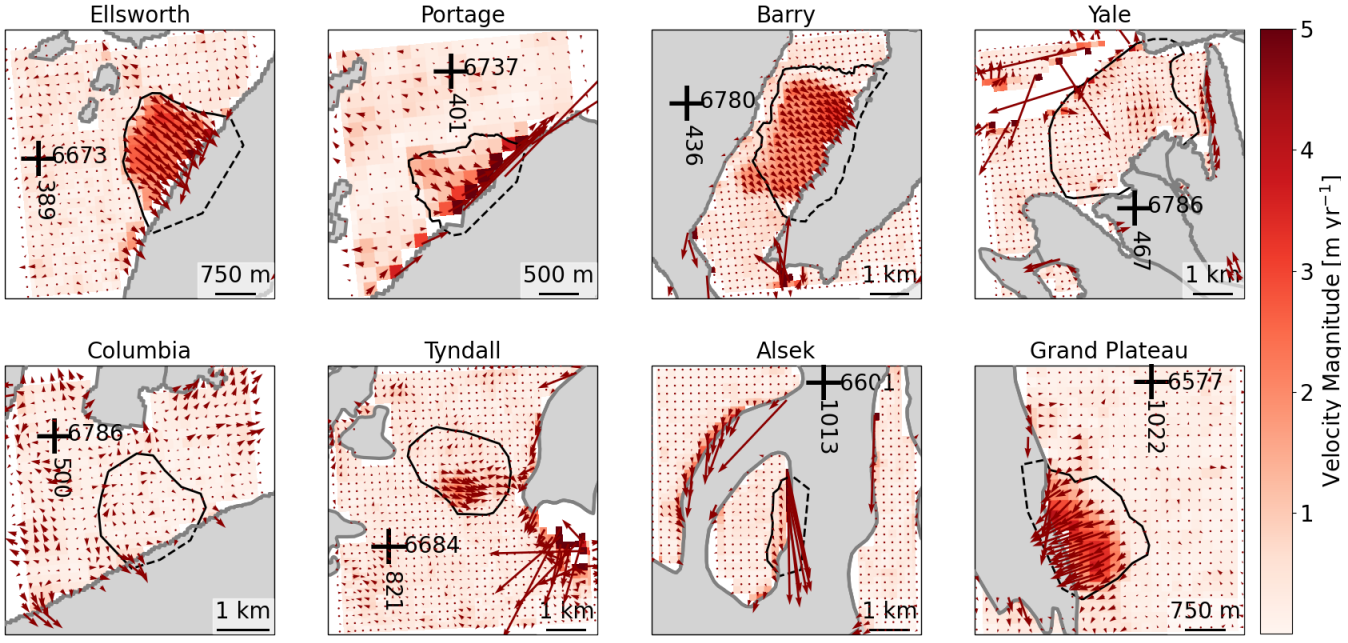

Figure 3. Average (1984-2022) displacement vectors and velocity magnitude derived from ITS-LIVE data. Glaciers are shown in gray (outlines from RGI Consortium, 2017) and black outlines mark the instability polygon (cf. Fig. 2). Coordinate crosses are given in UTM 6.

after this period, though the ITS-LIVE data indicates a small velocity increase around 2010 (see Fig. 4b1), which may suggest slight ongoing creep.

315 At four other sites (Barry, Grand Plateau, Alsek, and Ellsworth), activity started between 2000 and 2010. The Barry landslide accelerated between 2004 and 2010 (Fig. 4a1 and Fig. 6A). Manual feature tracking indicates the movement started between 2009 and 2010, while ITS-LIVE data shows the acceleration beginning after 2008 and the velocity peaking around $30\,\mathrm{m\,yr^{-1}}$ between 2010-2012. Between 2013-2016, the landslide slowed to around $10\,\mathrm{m\,yr^{-1}}$ before the velocity stabilized at approximately $2\,\mathrm{m\,yr^{-1}}$ in 2017. This acceleration displaced large parts of the landslide by around $200\,\mathrm{m}$ in total between 2004 and
320 2021. During the same time (beginning of the 2000s), a $\sim 45\,\mathrm{m}$-wide crack opened at the top of the Grand Plateau landslide (Fig. 4d1 and Fig. 6D). Manual feature tracking narrows down the movement onset to between 2007 and 2009. ITS-LIVE data reveal that slope-scale motion continued between 2010 and 2022, albeit movement appears to have stopped around 2018, with the exception of an active drainage area in the north. For both Barry and Grand Plateau glaciers, we observed small slope failures along one side of the valley as the glacier retreated up-valley.

325 At Alsek Glacier, the ITS-LIVE landslide velocity peaked at over $20\,\mathrm{m\,yr^{-1}}$ in 2008 and a $60\,\mathrm{m}$ wide crack opened between 2006 and 2008 (Fig. 4h1). After this event, only slight displacement (<$30\,\mathrm{m}$) occurred between 2010 and 2021. A similar phenomenon is observed at Ellsworth Glacier: The landslide accelerated dramatically in 2009, reaching velocities of over

https://doi.org/10.5194/egusphere-2024-1086
Preprint. Discussion started: 30 May 2024

$80\,\mathrm{m\,yr^{-1}}$ and a cumulative displacement of $100\,\mathrm{m}$ between 2005 and 2010 (see Fig. 4e1). Later, between 2014 and 2021, the landslide continued to move, giving displacements around $30\,\mathrm{m}$.

Finally, two sites had minimal-to-no movement over the study period. At Portage, no movement was detected by manual feature tracking (Fig. 4f1) albeit ITS-LIVE data indicates clear down-slope motion (Fig. 3). This suggests that there is slow but possibly continuous motion without any sudden, large changes. At Columbia, no motion could be detected by ITS-LIVE (Fig. 3) or by manual feature tracking (Fig. 4g1), despite the fact that the landscape shows signs of deformation.

4.2 Glacier evolution

All glaciers retreated between 1984 and 2022, with total retreat varying from 0.97 to $23.3\,\mathrm{km}$ and average retreat rates ranging from 30 to $630\,\mathrm{m\,yr^{-1}}$. Two sites also showed periods of advance, but the 2023 terminus positions are up-valley of the 1980s extents in all cases. In accordance with the observed retreat, all sites thinned between 1960 and 2020, with average thinning rates ranging from 1.77 to $9.65\,\mathrm{m\,yr^{-1}}$ (Tab. B1, as well as Fig. 5). At four out of eight sites, periods with rapid glacier changes coincide with periods of landslide activity and slope acceleration (Fig. 4 and Fig. 6).

Between 1984 and 1988, Tyndall Glacier retreated up-fjord by $5\,\mathrm{km}$. This rapid retreat coincided with the crack opening at the head of the landslide (Sect. 3.1), which appears to have occurred as the glacier terminus passed the landslide. Following this dramatic retreat, the glacier terminus advanced by around $700\,\mathrm{m}$ between 1995 and 2021. Near the landslide, the glacier thinned by $6.42\,\mathrm{m\,yr^{-1}}$ on average between 1960 and 2000, and thickened by $0.56\,\mathrm{m\,yr^{-1}}$ between 2000 and 2020 (Tab. B1). In our study, Tyndall and Yale are the only two glaciers that showed short phases of advance. Like Tyndall, Yale experienced times of modest advance (a maximum of $170\,\mathrm{m}$), around the year 2000 and after 2006 (Fig. 4b2). Despite these short phases of stability or advance, Yale Glacier retreated by around $1200\,\mathrm{m}$ since the 1980s, a trend that was accompanied by rapid thinning. On average, Yale glacier thinned by $3.29\,\mathrm{m\,yr^{-1}}$, the thinning rate being more than twice as high before the year 2000 than afterwards ($5.52\,\mathrm{m\,yr^{-1}}$ versus $2.18\,\mathrm{m\,yr^{-1}}$; Tab. B1). The increased thinning rate before 2000 also coincided with one of the most rapid periods of retreat: between 1989 and 1995, the glacier terminus retreated past the landslide area at around $70\,\mathrm{m\,yr^{-1}}$, which is more than twice the long-term retreat rate of $30\,\mathrm{m\,yr^{-1}}$. Again, the strong retreat coincided with the main landslide displacement.

Barry Glacier retreated most rapidly up-fjord between 2003 and 2016, and slope motion began between 2009 and 2010 when the terminus was adjacent to the down-valley margin of the landslide. During this period of accelerated retreat, the terminus retreated around $230\,\mathrm{m\,yr^{-1}}$, which was nearly three times higher than the average retreat rate over the 1985-2022 period. Near the landslide, the glacier thickened slightly ($0.87\,\mathrm{m\,yr^{-1}}$ on average) prior to 2000, while between 2000 and 2020 the thinning rate was the second highest of the study ($9.65\,\mathrm{m\,yr^{-1}}$; Figs. 4a2 and 5).

Similar to Barry, Grand Plateau Glacier also retreated around $3\,\mathrm{km}$ between 1985 and 2022, with the termini of both sites having retreated past most or all of the landslide. The thinning rates have been generally increasing since the 1980s. Near the landslide, the glacier thinning rate was $2.63\,\mathrm{m\,yr^{-1}}$ on average before 2000, and increased by a factor of two between 2000 and 2020. Since the 1980s, the retreat rate of Grand Plateau gradually accelerated as the glacier moved up-valley through the lake, but there was not one distinct period of acceleration. The glacier retreated around $90\,\mathrm{m\,yr^{-1}}$ on average between 2007

https://doi.org/10.5194/egusphere-2024-1086
Preprint. Discussion started: 30 May 2024

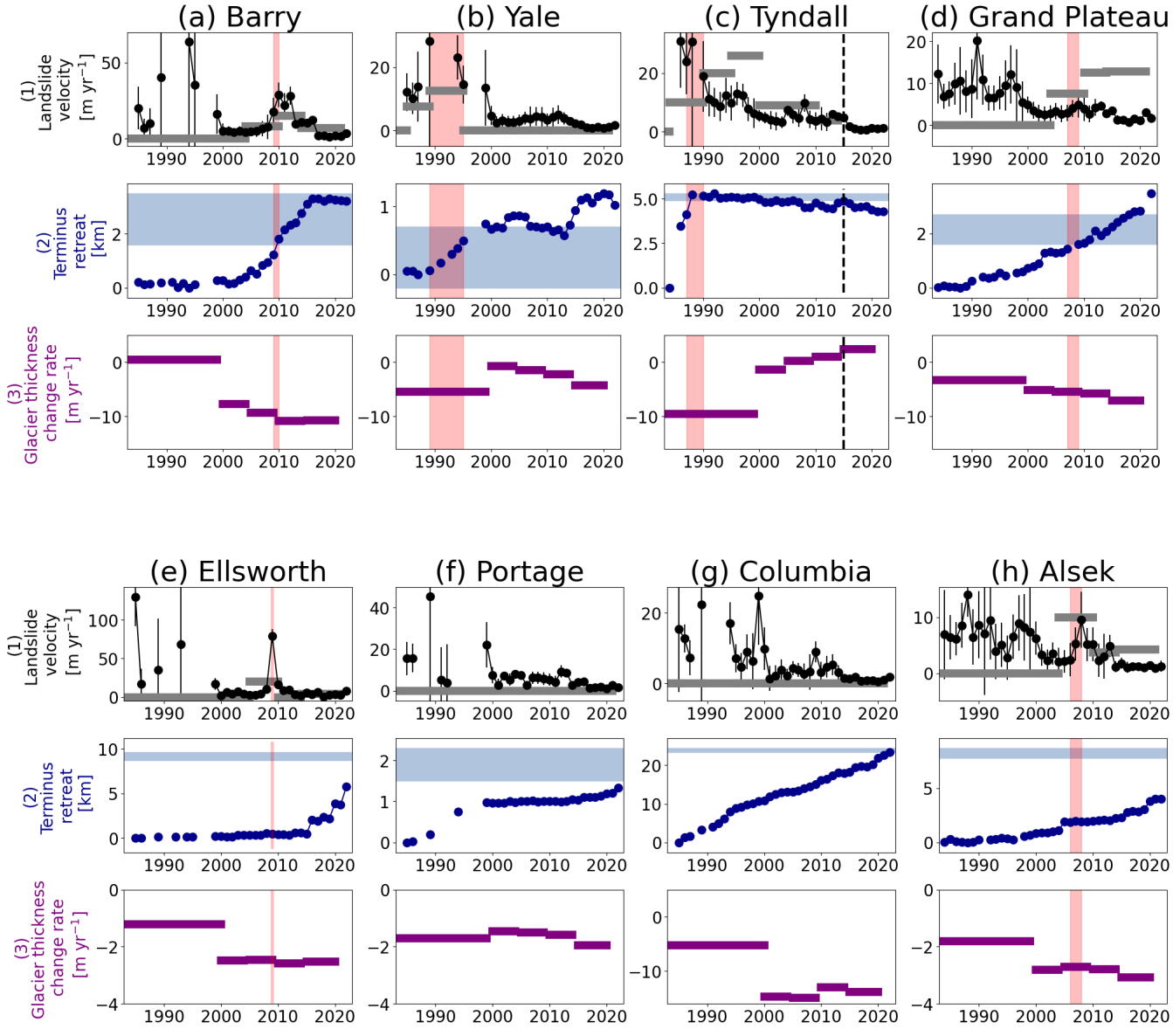

Figure 4. Landslide and glacier evolution at the sites of interest. Top row: Landslide velocities from ITS-LIVE (black circles, with vertical lines showing the uncertainty estimate from ITS-LIVE) and manual feature tracking (gray bars). Middle row: Terminus retreat (dark blue) and location of the landslide along the glacier centerline (light blue shading). Bottom row: Glacier thickness change rates within the IAG polygon (see Fig. 2 for definition) based on data from Dehecq et al. (2020) and Hugonnet et al. (2021). Note at Ellsworth and Columbia, the Berthier et al. (2010) DEM replaced the Dehecq et al. (2020) DEM. In all panels, light red shading indicates the onset of landslide movement. At Tyndall, the black dashed line indicates a catastrophic failure. Note the differing scales on the y-axis for the individual sites.

https://doi.org/10.5194/egusphere-2024-1086
Preprint. Discussion started: 30 May 2024

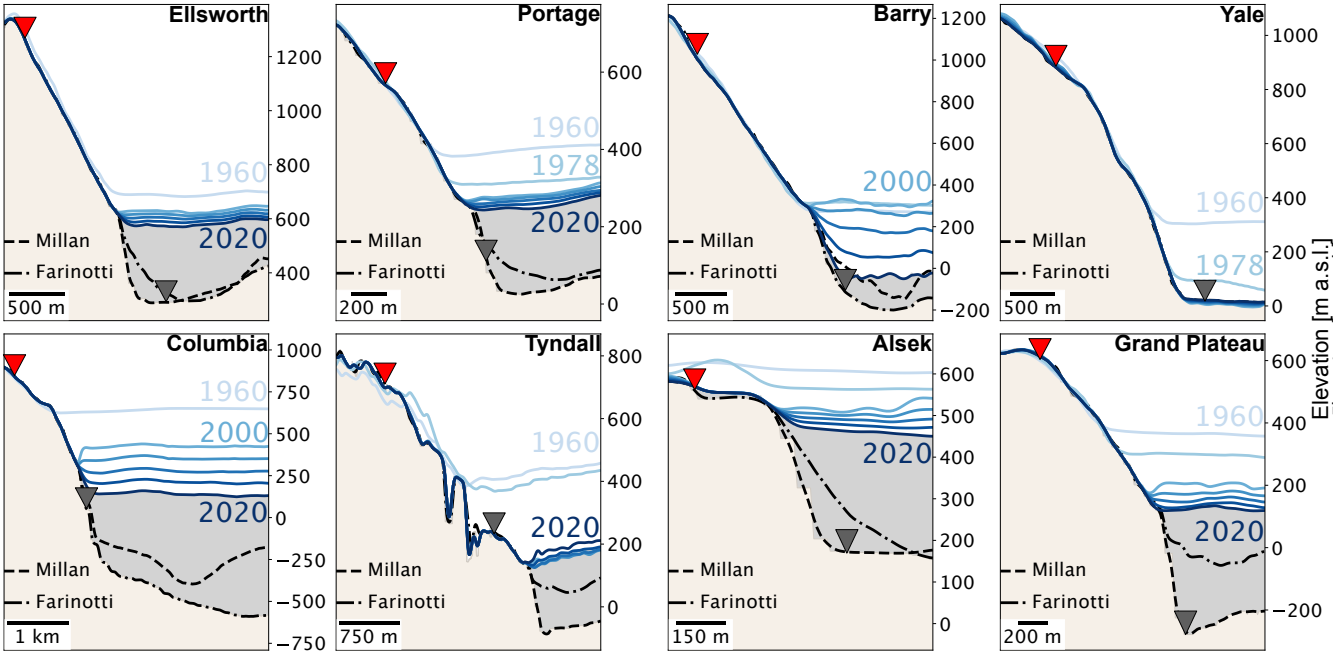

Figure 5. Cross sections through the landslide and glacierized area at each site. Bedrock (tan) and glacier areas (gray) are shown. Glacier surface elevations are plotted in progressively darkening shades of blue. Subglacial topography is given by two ice thickness datasets (Millan et al. (2022) and Farinotti et al. (2019)). Red and gray triangles mark the upper and lower bounds of the landslide, respectively. Note the horizontal and vertical scales vary between sites.

and 2009, coinciding with both the glacier passing the down-valley margin of the landslide and the opening of the crack (Sect. 4.1). During this period, the retreat rate was equal to the 1984-2022 average velocity.

At Ellsworth and Alsek glaciers, both the retreat and thinning rates have increased over time (Fig. 4). Next to the landslide, Ellsworth Glacier's thinning rate was $1.22\,\mathrm{m\,yr^{-1}}$ on average prior to 2000, which increased by a factor of two between 2000 and 2020 (Figs. 4e3 and 5). This corresponds to the time when the landslide accelerated. The position of the terminus was fairly stable in the proglacial lake until 2014, when the tongue of the glacier began disintegrating and led to higher retreat rates. However, the instability was still around $3\,\mathrm{km}$ from the terminus. Next to the landslide, Alsek Glacier thinned by $1.57\,\mathrm{m\,yr^{-1}}$ between 1960 and 2000, and by $2.85\,\mathrm{m\,yr^{-1}}$ between 2000 and 2020, a factor of 1.8 higher (Figs. 4h3 and 5). This brackets the period with the crack opening. Alsek Glacier's retreat through the proglacial lake followed a similar pattern: prior to 2000, the glacier retreated around $45\,\mathrm{m\,yr^{-1}}$ and the rate increased by a factor of three since then. However, the terminus is still about $4\,\mathrm{km}$ down-valley from the instability.

Both Portage and Columbia thinned during the study period, and the terminus is currently several hundred meters from the instability centerpoint (Fig. 4). With Tyndall and Yale, Portage Glacier is one of three sites where the thinning rate was higher before 2000 than it was afterwards: Portage thinned at $2.2\,\mathrm{m\,yr^{-1}}$ before 2000, and at around $1.62\,\mathrm{m\,yr^{-1}}$ between 2000 and

https://doi.org/10.5194/egusphere-2024-1086
Preprint. Discussion started: 30 May 2024

2020. The glacier retreated rapidly ($65\,\mathrm{m\,yr^{-1}}$) through the proglacial lake between 1985 and 2000, remained stable for around 15 years, and retreated at around $40\,\mathrm{m\,yr^{-1}}$ since 2015. Columbia Glacier, on the other hand, thinned by $5.2\,\mathrm{m\,yr^{-1}}$ on average between 1960 and 2000, increasing by a factor of 2.7 to $14.1\,\mathrm{m\,yr^{-1}}$ between 2000 and 2020. Here, steepening of the slope, likely due to glacier erosion, is clearly visible below the 1960s glacier surface (Fig. 5). Between 1985 and 2022, the glacier retreated up-fjord by over $23\,\mathrm{km}$, or a rate of around $630\,\mathrm{m\,yr^{-1}}$.

4.3 Landslide-glacier interaction

At four sites (Tyndall, Yale, Barry, Grand Plateau), we observed that landslide deformation began or increased as the glacier terminus passed the active area of the landslide. At Tyndall Glacier, the very rapid terminus retreat debuttressed the landslide within a period of three years and a crack opened at the top of the slope when the glacier passed the landslide toe (Fig. 6C). A crack also formed at Grand Plateau landslide where, as the terminus retreated past the down-valley margin of the landslide, slope-wide deformation began (Fig. 6D). The same is true for Barry Glacier: when the terminus was adjacent to the down-fjord edge of the instability, the whole slope moved significantly and a headscarp formed (Fig. 6A). At Yale Glacier, the movement was more localized and involved only the active area rather than the entire instability, but the surface features displaced down-slope as the terminus passed the active area (Fig. 6B).

At the four sites where the terminus is still down-valley with respect to the instability (Portage, Ellsworth, Alsek, Columbia), we see varying behavior of the landslides. At Portage Glacier, the landslide moved slightly, but with a constant velocity and without a distinct acceleration. At Ellsworth and Alsek, the landslides had sudden, large accelerations that do not coincide with an obvious change in the glacier. However, the glacier thinning rates of both sites increased by about a factor of two over the same period as the landslide accelerations. On the contrary, thinning at Columbia Glacier increased by a factor of almost three but no landslide deformation was observed. While the link between glacier changes and landslide evolution is less clear at these four sites, we suggest that it could be related to glacier thinning.

4.4 Landslide-environment interaction

The results presented in the sections above suggest that glacier changes, especially rapid retreat, may exert a strong control on landslide acceleration. To make this inference, however, alternative factors that might have initiated the larger slope displacements need to be ruled out. Here below we address meteorology and seismicity as potential alternative explanations.

4.4.1 Meteorology

Annual precipitation does not reveal any trend during the 1979-2022 time series. All sites have relatively large precipitation totals, on average around $3200\,\mathrm{mm\,yr^{-1}}$. The mean annual air temperature increased between 1979 and 2022 at all sites, on average by $0.04\,^{\circ}\mathrm{C\,yr^{-1}}$.

We examined the cumulative monthly precipitation at the six sites which experienced landslide accelerations (Fig. 7). At Ellsworth, where the landslide accelerated between June and August 2009, yearly precipitation was below average. However,

https://doi.org/10.5194/egusphere-2024-1086
Preprint. Discussion started: 30 May 2024

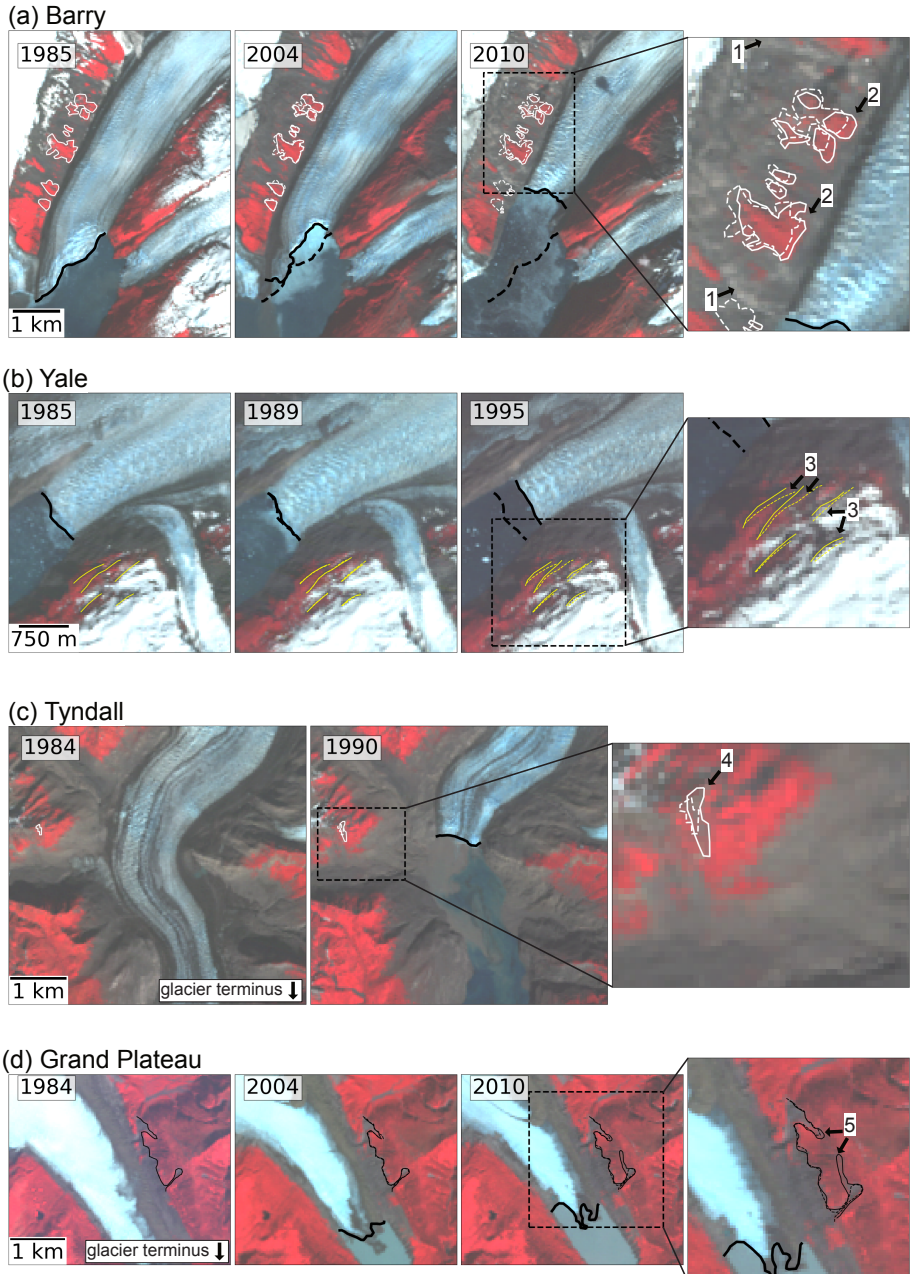

Figure 6. Landslide features and glacier terminus position during movement onset for sites where the terminus has passed the landslide. The year of acquisition of the individual satellite images is given at upper left. The panel at far right shows a zoomed version of the previous panel (shown by the black dashed box). Solid lines refer to the year at upper left in each image and for subsequent years, dashed outlines refer to the first time period (image at far left). Arrows highlight the formation of a head scarp (1), downward displacement of vegetation patches (2), downward displacement of surface features (3), widening of a crack (4), and the formation of a crack (5). Panels A-D refer to Barry, Yale, Tyndall, and Grand Plateau, respectively. Background images are Landsat 4-7 courtesy of the U.S. Geological Survey.

https://doi.org/10.5194/egusphere-2024-1086
Preprint. Discussion started: 30 May 2024

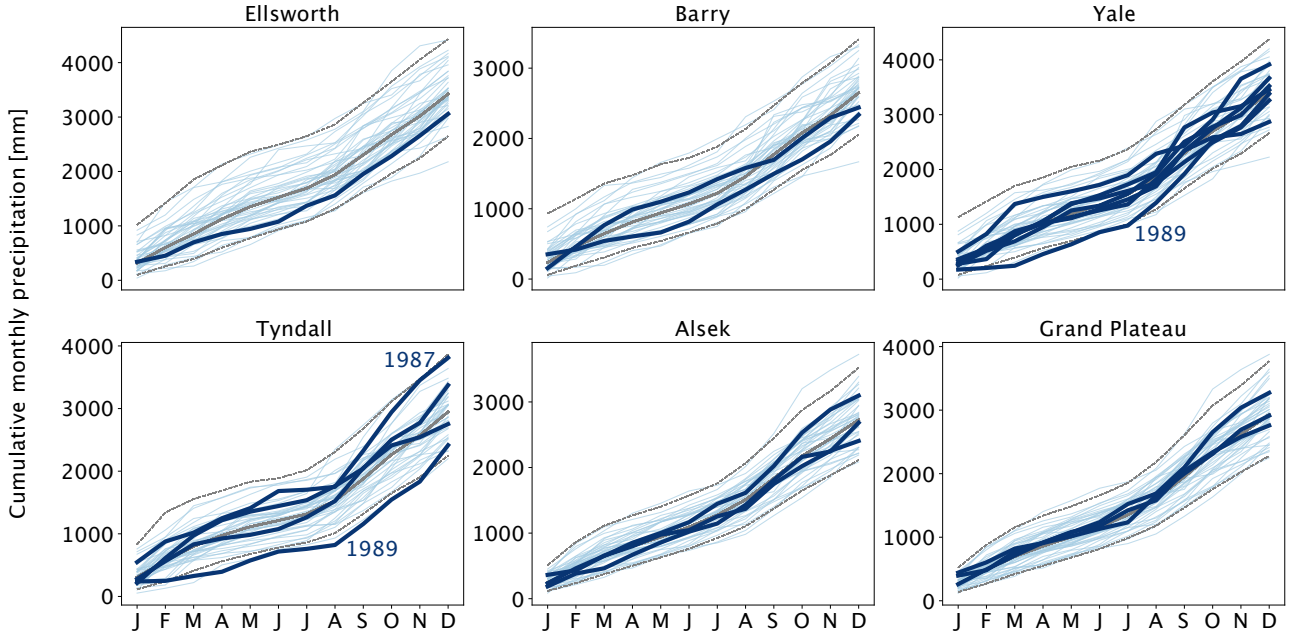

Figure 7. Cumulative monthly precipitation at all sites which experienced a landslide acceleration during the study period. Thicker, darker blue lines correspond to the year (or years) during which the landslide accelerated. The light blue lines are all other years. The solid gray line corresponds to the mean monthly precipitation over the whole time period, and the gray dashed lines are two standard deviations above and below the mean. Note that y-axes differ between sites.

the precipitation during July 2009 was as high as 293 mm, which is 80% above the average precipitation for July (Fig. D1). A connection between precipitation and landslide acceleration can thus not be ruled out in this case.

At Barry, Alsek, and Grand Plateau glaciers, precipitation totals during the years of the landslide acceleration were close to the long-term average. At Yale and Tyndall glaciers, one year during the landslide acceleration period (1989) was exceptionally dry, particularly in the first half of the year. At Tyndall, precipitation totals were well above average in November and December of 1987. Because we cannot determine the onset of the landslide movement more precisely, it is unclear if the acceleration might be related to this large precipitation amount or if it happened during a different time of the year. Since it is fair to assume that the November and December precipitation fell as snow, one hypothesis could be that the landslide might have experienced increased loading. Taken together, however, the indications for a direct link between precipitation and landslide movement are weak.

4.4.2 Seismicity

The seismic data were scrutinized to determine whether slope accelerations followed intense or prolonged seismic activity. At four sites (Ellsworth, Barry, Yale, Tyndall), the landslide accelerations occurred during a period of low seismicity (Fig. 8). At Alsek Glacier, a small earthquake occurred during the same time period as the landslide acceleration. The onset of movement

https://doi.org/10.5194/egusphere-2024-1086
Preprint. Discussion started: 30 May 2024

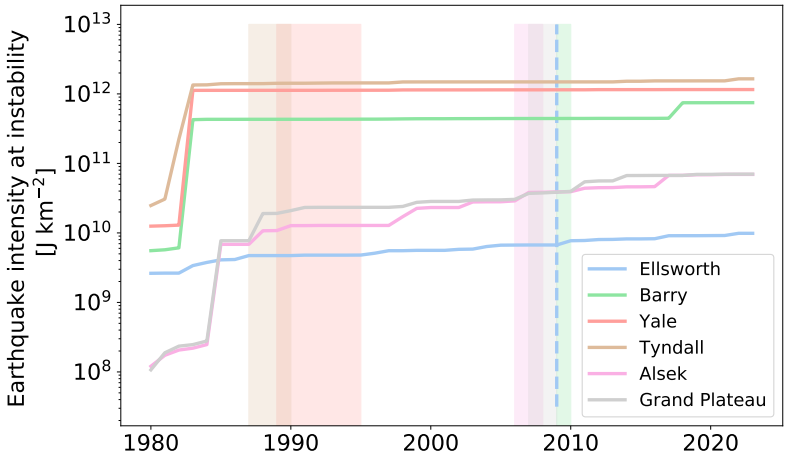

Figure 8. Seismic intensity at the sites which experienced a landslide acceleration during the study period. For Ellsworth, where the acceleration can be pinpointed to a single year, that year is marked by a vertical dashed line. For other sites, the instability acceleration is marked by a shaded bar.

at Grand Plateau Glacier appears to occur shortly after a small increase in earthquake intensity. Due to limited availability of satellite images, we cannot precisely constrain the onset of the landslide movement and thus do not know if a link might exist. However, both sites experienced even larger increases in seismic intensity in previous decades without leading to landslide movement, which seem to speak against a possible causal link. We note that at most sites, large earthquakes occurred between 1980 and 1988. While these may have preconditioned the slope stability though fracturing, a clear link cannot be established.

5 Discussion

In this study, we investigated the response of paraglacial landslides to glacier changes over multiple decades. Our results show that in four of eight cases (Yale, Tyndall, Grand Plateau, Barry; all of which are lake- or marine-terminating glaciers), the landslides accelerated when the glacier retreated past the instability. Ellsworth experienced an increase in glacier thinning, but the landslide acceleration also coincided with an anomalously rainy month. At Alsek, we found a sudden activation which was preceded by an increase in glacier thinning. Finally, despite the continuous mass loss of both glaciers, Portage showed very little movement without a clear period of acceleration, and at Columbia, no movement was detected.

The impact of glacier thinning on landslide destabilization has been investigated at several locations across the world, and there is general agreement that glacier thinning contributes to landslide destabilization (e.g., McColl and Davies, 2013; Lacroix et al., 2022; Glueer et al., 2019; Cody et al., 2020). So far however, most studies investigating glacial debuttressing have taken place at sites where the glaciers were land-terminating. Observations of landslides adjacent to lake- or marine-terminating glaciers are much less common (an exception is given by the studies of Kim et al. (2022) and Dai et al. (2020)), as is documentation of accelerations at such sites. In the following, we discuss possible differences between the land- and

https://doi.org/10.5194/egusphere-2024-1086
Preprint. Discussion started: 30 May 2024

water-terminating situations, evaluate the varying slope evolutions following destabilization, and address the limitations of our methods. We also compare our results to previously published work and propose future research perspectives.

5.1 Landslide activation mechanisms

Examining landslide and glacier evolution over several decades allowed us to determine the timing of what we refer to as landslide *activation*. It is possible and indeed probable that the underlying structures of these landslides have existed for many decades, centuries, or even millennia, and previous work has shown that landslides can reactivate or even fail millennia after deglaciation (Hermanns et al., 2017). We thus do not speak about landslide initiation, nor do we rule out that earlier phases of activity may have existed, meaning that the displacements we observed are actually ones of a reactivation. Instead, we use the term *activation* to indicate the onset of detectable movement during our study period.

When trying to establish a mechanism relating glacier mass loss to the observed instabilities, our sites can be divided into two categories: those where the glacier terminus has already retreated beyond the landslide, and those where the terminus is still downstream of the landslide. We will refer to landslides in the former case as being impacted by "retreat-related" debuttressing, and as "thinning-related" debuttressing in the latter case. We acknowledge that glacier retreat and thinning are closely linked, meaning that the processes cannot be fully separated, but we use these terms to distinguish between slopes which have undergone a complete loss of glacier support from slopes in which some glacier buttressing is still present.

At Yale, Tyndall, Grand Plateau, and Barry, we observed a sudden activation of the landslides in response to rapid glacier retreat. In all four cases, the glaciers retreated past the landslides through lakes or fjords, and at rates up to 12 times their long term average. Marine- and lake-terminating glaciers can retreat more rapidly in comparison to land-terminating glaciers due to feedback processes between ice dynamics and submarine topography. In particular, a combination of warm water intrusion (Weertman, 1974), dynamic thinning, and surface melt can cause the calving front to thin beyond the flotation level, thus causing rapid retreat though calving (Epprecht, 1987; Cuffey and Paterson, 2010). Since the calving rate is proportional to water depth, the retreat is fostered in places with deeper water (Hanson and Hooke, 2000).

Such rapid, calving-driven retreat also means that at the corresponding locations, the landslide-ice interface is replaced with a landslide-water interface. The concomitant changes in water saturation of the landslide toe, together with structural changes induced by the redistribution of mechanical stresses as the landslide support changes from glacier ice to water, may partially explain the susceptibility of these slopes to sudden activation. Indeed, we hypothesize that such changes in boundary conditions are generally faster in the case of a rapidly retreating lake- or marine-terminating glacier than they are at land-terminating glaciers, which may make a landslide activation more likely in the former case. Beyond this faster change, we believe there are several other relevant differences between this retreat-related situation and its thinning-related counterpart.

As a marine- or lake-terminating glacier retreats past a landslide toe, the forces acting upon the slope change significantly. In particular, the glacier provides buttressing support to the landslide prior to retreat. Although ice can deform at very low strain rates (McColl and Davies, 2013), the buttressing is more pronounced that the one provided by water after glacier retreat. This change occurs suddenly, owing to the vertical cliffs that are characteristic of calving fronts (Cuffey and Paterson, 2010)

https://doi.org/10.5194/egusphere-2024-1086
Preprint. Discussion started: 30 May 2024

and their fast retreat due to calving. This may lead to localized structural changes within the landslide area, which might cause additional, slope-scale redistribution of mechanical stress as the landslide mass starts to deform.

The other primary change relates to the hydrologic conditions at the landslide toe. Existing work indicates that during ice sheet retreat, groundwater exfiltrates from the subsurface due to the decrease in ice overburden pressure while ice loading can lead to ground compaction and the closing of fractures in the subsurface (Ravier and Buoncristiani, 2018). If the reverse were true, i.e. if fractures open upon ice unloading, increased infiltration could occur after glacier retreat. This would in turn lead to increased pore water pressure, which was found to be positively correlated to landslide movement (McColl, 2015). Regardless of the direction of the subsurface fluxes, hydraulic gradients caused by groundwater fluctuations can impact slope stability (McColl, 2015), and the change from a landslide in contact with ice to a landslide in contact with water will undoubtedly alter these gradients.

For landslides near the termini of marine-terminating glaciers, tidal forces may also play a role in the destabilization. Prior to complete glacier debuttressing, the glacier ice would largely protect the landslide from both tides and waves. Once the glacier has retreated, the slope would become vulnerable to both cyclical tidal forces and wave action. Together, these processes may cause increased erosion and rearrangement of sediment, which can in turn impact landslide stability (Doi et al., 2020). The increased erosion might also reinforce itself, as the released materials can further increase abrasion (Payo et al., 2016), thus further affecting the overall landslide stability.

The above considerations suggest that landslides adjacent to rapidly retreating lake- or marine-terminating glaciers may be particularly susceptible to activation. However, various forms of landslide activity were also detected for sites that "only" experienced thinning. At both Ellsworth and Alsek, for example, landslide activation occurred 6 to 8 years after glacier thinning increased by a factor of $\sim$2. Lacroix et al. (2022) made a similar observation for Iceland, where a landslide acceleration followed 6 years after a marked increase in glacier thinning rate. One hypothesis is that landslide activation begins after the glacier ice thins to a critical thickness. For the Moosfluh landslide in Switzerland, for example, Storni et al. (2020) found that slope displacements were higher where ice thickness was below $50\,\mathrm{m}$ and smaller where the ice was ca. $100\,\mathrm{m}$ thick, while Glueer et al. (2019) found that the whole landslide accelerated after the ice thickness thinned below $100\,\mathrm{m}$. Our results instead show that the landslide accelerations at Ellsworth and Alsek occurred when the local ice thickness was still in the order of 300 m (Ellsworth) to 350 m (Alsek), indicating that such thickness thresholds are site specific. Taken together, thinning-related debuttressing does not seem sufficient to explain all of the observed landslide behavior, and indeed, the Portage landslide deformed continuously as the glacier thinned while no acceleration was seen at Columbia despite an increase in glacier thinning rate by a factor of 2.7

Precipitation might be a further cause of landslide activation, in addition to glacier changes. In one case (Ellsworth, cf. Sect. 4.4.1), we found above-average July precipitation coinciding to landslide acceleration, although the precipitation total in July was lower than typical autumn amounts. This indicates that the total precipitation was not unusual for the site, while the timing was. This could be relevant for two reasons. First, the available temperature data indicate that the precipitation likely fell as rain in July and as snow in autumn (Fig. D2). Second, the subsurface may have been additionally saturated from ice melt in

https://doi.org/10.5194/egusphere-2024-1086
Preprint. Discussion started: 30 May 2024

summer. Together, these conditions could have led to above-average pore water pressure and thus, to the observed landslide acceleration. Being based on observations of one site only, however, we recognize the such a mechanism remains speculative.

Also the relation between seismic activity and landslide activation remains inconclusive. Our study period began in 1980, 16 years after a magnitude 9.2 earthquake rocked Alaska (Kanamori, 1977), and it is not excluded that such a large seismic event might have weakened the various slopes through mechanical damage without causing instantaneous failure. In an analysis focusing on central Italy, for example, Song et al. (2022) found that landslide accelerations occurred in areas with light-to-moderate ground-shaking. This is in line with findings by McColl (2015), who noted that i) landslides can withstand many dynamic events (such as due to seismic activity) without failing and ii) the event triggering catastrophic failure may not be the largest. While we do not find a direct link between seismic activity and slope accelerations in our data, we still suggest that seismic events can contribute to the development of instabilities through a preconditioning of the related slopes.

5.2 Evolution following landslide activation

Our results show that the initial landslide response to glacier retreat does not determine the long-term evolution of the landslide. In particular, both re-stabilization and catastrophic failure might occur. At Yale, for example, no further movement followed after the landslide activation in the early 1990s. This is different from what was observed at Barry and Grand Plateau, where measurable deformation continued after activation. Barry accelerated rapidly and then slowed, while Grand Plateau moved at a constant, accelerated pace. Tyndall, instead, is an example for a landslide that evolved to catastrophic failure.

Once the glacier retreats past the landslide, it can no longer be the factor controlling landslide displacements. Hydro-geologic mechanisms must become dominant. An example of these changing controls is the situation at Barry, where a head scarp was already visible in 1957 imagery of the U.S. Air Force, indicating that the landslide was active prior to the acceleration in the early 2000s. We do not know how long the head scarp persisted, nor what caused its original formation. However, our analyses and the findings of Dai et al. (2020) suggest that glacier retreat was an important mechanism as the terminus passed the landslide toe. The idea that the controlling mechanism can change over time (see also Schaefer et al., 2023, for the Barry case), means that periodic assessments are necessary to understand and address the evolving hazard.

In cases where the terminus has not yet retreated past the landslide, the question remains about what will happen when that occurs. One hypothesis is that the landslides will reach a new equilibrium as the glaciers thin and the slopes (re-)adjust to the changed boundary conditions. Another hypothesis is that thinning-related debuttressing will cause critical weakening of the slopes, eventually leading to landslide acceleration. While our results let us favor the latter hypothesis, it remains unknown if such accelerations will eventually also increase the chances for future slope failure.

5.3 Methodological limitations

In this work, we relied on ITS-LIVE as one source of landslide displacement velocities. The dataset was originally designed for quantifying glacier flow velocities, so the processing parameters are optimized for velocities that are much higher than for typical landslide motion. The coarse resolution of the dataset also means that small displacements cannot be detected accurately. ITS-LIVE is thus expected to perform better for larger and fast-moving landslides, where surface features and

https://doi.org/10.5194/egusphere-2024-1086
Preprint. Discussion started: 30 May 2024

resulting displacements are larger. The same is true for displacements measured by manual feature tracking, where we expect that the minimum measurable displacement is around two pixels, i.e. $60\,\mathrm{m}$. Small changes or displacements of landslide are by no means irrelevant, but the resolution provided by both the feature tracking datasets seem adequate for investigating the slope-wide responses of the landslides to glacier changes.

In some areas, the ITS-LIVE data also appears to show some "leakage" of the glacier signal to glacier-adjacent pixels. This is especially apparent at Portage Glacier, where several pixels classified as non-glacier have very high velocities and move parallel to the glacier (Fig. 3). This may result from i) uncertainties in the glacier margins, ii) temporal inconsistencies between the glacier margins and the ITS-LIVE data, or iii) a large window size used during the process of image cross correlation. This leaked signal typically extends 1 to 2 pixels (i.e. up to $240\,\mathrm{m}$) away from the glacier and thus affects a small portion of the landslides' extents. We do not expect this leakage to impact our results, however, as we only compute velocities within a defined "active area" (see Sect. 3.1). The confidence in the methods used here is further increased by the good agreement between ITS-LIVE derived displacements and existing work at Barry Glacier (see Sect. 5).

To determine the importance of the glacier changes, we also analyzed time series of precipitation. However, determining an appropriate time scale for such an analysis is challenging, as landslides can be activated by both heavy precipitation events of short duration as well as extended periods of particularly wet conditions. Indeed, existing literature shows that landslides can respond to a wide range of precipitation totals, both in wet and dry climates (Handwerger et al., 2022), and on timescales ranging from minutes to several months (Iverson, 2000; McColl, 2015). Similarly, there is evidence for the interannual precipitation changes to play a role, with a number of landslides being initiated during a rainy year following a drought (Handwerger et al., 2019). The landslide response to precipitation also depends on the local geology, the specific characteristics of the instability, as well as the local topography and hydrology (Lacroix et al., 2020). Lacroix et al. (2020) states that elevated landslide velocities are typically seen during i) periods with intense precipitation, ii) times with long-lasting precipitation, or iii) the melt season. For our analysis, we chose to investigate temporal resolutions that are consistent with the available information on glacier and landslide changes, acknowledging that by doing so we cannot capture the full variability of the meteorological processes.

There are several additional factors which we did not consider in this work. For example, the site-specific structural geology, such as the composition of the landslide and the fracturing of the subsurface, is undoubtedly a critical factor for slope stability. The subsurface properties cannot be determined without intensive field studies, but such studies are not feasible at the regional scale studied here. Similarly, we did not consider any specific information on the slopes' hydrology, as such information is simply not available. Lastly, we did not explicitly consider snow heights, as we expect this factor to be correlated with precipitation.

5.4 Comparison to previous works

Existing work at five of the eight sites has independently confirmed landslide movement. Schaefer et al. (2024) found average line-of-sight speeds ranging from 0.41 to $9.64\,\mathrm{mm\,yr^{-1}}$ for Ellsworth, Portage, Barry, Yale, and Columbia. These values are very different from the ones obtained in this work, which we attribute to the differing methods used, as well as different periods of investigation. While Schaefer et al. (2024) used InSAR data, which measures small displacements but may not be

https://doi.org/10.5194/egusphere-2024-1086
Preprint. Discussion started: 30 May 2024

Table 1. Comparison of landslide velocity at Barry Glacier from Dai et al. (2020) and this work. The 'Ratio' is computed by dividing the value from this work by the value from Dai et al. (2020).

Time Period	Dai et al. (2020) $[\mathrm{m\,yr^{-1}}]$	This Work $[\mathrm{m\,yr^{-1}}]$	Ratio [–]
1999 - 2008	1.3 ± 0.6	6.4 ± 4.8	4.9
2010 - 2013	26 ± 3	22.2 ± 6.0	0.9
2014 - 2016	10 ± 2	11.3 ± 1.7	1.1
2017 - 2020	1.3 ± 1.7	1.7 ± 0.2	1.3

suitable for large accelerations (Manconi, 2021), we employed lower resolution satellite data. Additionally, Schaefer et al. (2024) investigated the period 2016-2022, and we characterized the long-term landslide evolution over a 40-year period. Of the 43 sites investigated by Schaefer et al. (2024), 11 were assessed as having the potential to generate a tsunami, and four of those 11 sites are also studied here. Regardless of the drivers, landslide movement and accelerations observed near deep lakes or fjords have important hazard implications.

In-situ measurements at Portage and Columbia have also confirmed movement at those sites. Deformation up to $5\,\mathrm{m}$ at the Portage landslide is visible in high-resolution digital image correlation between 2022 and 2023 (Lemaire et al., 2023b). This is somewhat higher than the $2.12\,\mathrm{m\,yr^{-1}}$ detected by ITS-LIVE on average over 2021-2022 (Fig. 4f1). At Columbia, movement on the order of several centimeters per year has been detected using GPS (B. Higman, personal communication) and InSAR (M. Jacquemart, personal communication). The discrepancy between these numbers and our results can easily be explained by the resolution of the satellite imagery (see Sect. 5.3).

At Barry, Dai et al. (2020) characterized the landslide movement since 2000 using feature tracking. A comparison to our ITS-LIVE results shows generally good agreement in terms of both timing of acceleration and average velocity magnitudes, the largest differences being found in the period 1999-2008, when the uncertainty is also largest, and the smallest differences being found in the periods 2010-2013 and 2014-2016 (Table 1). In their analysis, Dai et al. (2020) used imagery from Landsat (as we did), but also from ASTER, WorldView-1, and Ikonos, which have partly much higher resolution. This may explain some of the discrepancies.

5.5 Future research perspectives

Our study suggests that the rapid retreat of lake- and marine- terminating glaciers can lead to the sudden activation of paraglacial landslides. Since the retreat rate in such cases is related to water depth (as deeper waters imply enhanced calving), this raises the question whether landslide activation is preferentially co-located with deeper-than-average sections of lakes or fjords. Accurate bathymetric data would help answering this question, as they provide a detailed picture of the submarine environment adjacent to the landslides. If such a relation between water depth and landslide activation exists, ice thickness datasets as used in this work (Farinotti et al., 2019; Millan et al., 2022) could be used to estimate the up-valley extent of the lakes or fjords and thus

https://doi.org/10.5194/egusphere-2024-1086
Preprint. Discussion started: 30 May 2024

potential future water depths. This would be informative from a hazards perspective, also because the velocity of a potential tsunami triggered by a landslide collapsing into water is known to be proportional to water depth (Okal, 1988).

In terms of mechanistic understanding of the processes at play during landslide activation, the four cases where rapid glacier retreat coincided with landslide activation are obviously not sufficient to establish conclusive causalities. Broader regional studies with a focus on paraglacial landslides adjacent to lake- or marine-terminating glaciers would be helpful in this respect. At a more local level, detailed observations at sites where the glacier terminus is projected to soon pass the landslide area (e.g. Portage and Columbia) could yield valuable insights into the changing boundary conditions. Together, such regional and local studies could also help in further testing our framework distinguishing retreat- versus thinning- dominated debuttressing.

As glaciers continue to retreat and expose new fjords and lakes, the proximity of instabilities to water will change. This will have consequences in terms of hazard disposition and possible mitigation measures. We argue that additional observations would be useful in order to monitor known landslides and detect newly forming instabilities in a timely manner. Together, this may help to minimize the risk that a rapidly evolving environment poses to the public.

6 Conclusions

This work provides a regional overview of glacier debuttressing-related instabilities in southern coastal Alaska. We selected eight large landslides which are currently in contact with a glacier or have been so in recent decades, and which show signs of recent activity. At all sites, we use feature tracking in combination with glaciological, meteorological, and seismological datasets to examine correlations between slope movement and environmental changes between the 1980s and present-day. To extract slope velocities, we primarily use the ITS-LIVE dataset. While this dataset has fairly coarse resolution (120 m) and was originally designed for quantifying glacier flow velocities, comparison with in-situ observations (Dai et al., 2020) attest the suitability of the dataset for our purposes.

We find that the six out of the eight sites underwent significant slope acceleration at some stage during the studied time period. At four sites, such an acceleration occurred as the glacier terminus retreated past the landslide area. In these cases, the landslides border deep water bodies and we suggest that they underwent rapid debuttressing as the glacier retreated up-valley. For another two sites, landslide acceleration either coincided with a particularly rainy month, or with a significant increase in glacier thinning. The remaining two sites instead showed either slow, constant movement without a specific period of acceleration, or no detectable movement at all. In terms of causality, we hypothesize that the landslide accelerations were related to a loss of mechanical support from the glacier and to changes in the landslide hydrology. For the marine-terminating cases, we furthermore suspect that tidal forces eroding the landslide toe may have played a role.

The presence of large, unstable slopes poses a significant hazard, particularly when located in the vicinity of deep water. The rapid ongoing glacier retreat could expose more such slopes in future, potentially increasing the risk for some of these to fail catastrophically. In this context, we see two potential avenues for further work: First, more detailed investigation of the sites would be enlightening, since only limited information can be gained from a regional perspective. In-situ monitoring, for example, would provide more reliable data than available via the ITS-LIVE results, as well as a more complete picture of the

https://doi.org/10.5194/egusphere-2024-1086
Preprint. Discussion started: 30 May 2024

local processes. This is particularly important at sites that will experience debuttressing in coming decades, such as Portage or Columbia. Second, we see potential in using the ITS-LIVE data for detecting landslide events at the larger, potentially worldwide scale. Some aspects, such as the detection limits of the method and the leakage of the glacier signal to neighboring areas, would need to be addressed for that, but could lead to the early detection and monitoring of landslides at the regional scale. On the longer term, such a development could assist in dealing with the hazards that stem from a rapidly changing environment.

Code and data availability. Please contact the first author regarding the availability of code and data used in this work.

Video supplement. Videos showing the landslide activation at four sites are available as supplementary material.

https://doi.org/10.5194/egusphere-2024-1086
Preprint. Discussion started: 30 May 2024

Appendix A: DEM Years

Table A1. Summary of the years for which a DEM is available at the sites of interest. "BER" and "DEH" refer to the DEMs of Berthier et al. (2010) and Dehecq et al. (2020), respectively. Note that for the Dehecq et al. (2020) DEMs, multiple elevation models within a year may have been merged to generate the final product.

Name	Year (BER)	Year (DEH)	Notes (BER)
Ellsworth	1950	-	
Portage	1950	1980	
Barry	1957	1979-80	
Yale	1957	1979-80	
Columbia	1957	1979	
Tyndall	1972	1977	very small portions in the accumulation area are from 1974 or 1976
Alsek	1948	1977-78	
Grand Plateau	1948	1977-78	a portion of the accumulation area is from 1987

https://doi.org/10.5194/egusphere-2024-1086
Preprint. Discussion started: 30 May 2024

Appendix B: Glacier characteristics

Table B1. Glaciological characteristics of each site. "$\Delta H_{gl,X}$" is the median elevation change of the glacier within the instability-adjacent glacier polygon (see Sect. E and Fig. 2 for definition), where X is either 1 for the period 1960-1978, 2 for 1978-2000, or 3 for 2000-2020. Note that i) the values for $\Delta H_{gl,1-2}$ for Ellsworth and Columbia refer to the period 1960-2000, and ii) the values for $\Delta H_{gl,3}$ are an average of the 2000-2005, 2005-2010, 2010-2015, and 2015-2020 changes. "$H_{gl,F}$" and "$H_{gl,M}$" are the median thicknesses of the glacier within the instability-adjacent glacier polygon from Farinotti et al. (2019) and Millan et al. (2022), respectively.

	Ellsworth	Portage	Barry	Yale	Columbia	Tyndall	Alsek	Grand Plateau
$\Delta H_{gl,1}$ [m a^{-1}]	-1.22	-2.7	1.25	-5.61	-5.2	-3.29	-1.33	-1.97
$\Delta H_{gl,2}$ [m a^{-1}]		-1.7	0.48	-5.42		-9.55	-1.81	-3.3
$\Delta H_{gl,3}$ [m a^{-1}]	-2.51	-1.62	-9.65	-2.18	-14.1	0.56	-2.85	-5.85
$H_{gl,F}$ [m]	220	170	230	210	660	120	260	480
$H_{gl,M}$ [m]	250	200	280	260	400	240	280	260

https://doi.org/10.5194/egusphere-2024-1086
Preprint. Discussion started: 30 May 2024

Appendix C: Landslide volume

In order to determine landslide volume, it was first necessary to determine the landslide extent. We delineated a polygon from high-resolution imagery or lidar by selecting all topographic features that showed signs of deformation. Then, landslide volume was determined in two different ways: empirically and by expert estimation. We used an empirical relationship between the landslide surface area A_S and its volume V of the form

$$V = k \cdot A_S^{\beta}, \tag{C1}$$

where k and β are two empirical coefficients. We used three different sets of coefficients corresponding to a worldwide average for landslides, a worldwide average excluding shallow and submarine landslides, and an average for large landslides (Tab. C1). In addition, we completed expert estimation using the instability polygon and by inferring a sliding surface. To do so, the angle of the head scarp was extrapolated into the subsurface where available, and a concave failure plane was assumed in each case. We then estimated the volume between the basal failure plane and the surface.

Table C1. Different β and k coefficients used for estimating the volume of the instabilities V based on the instabilities' surface area A_S (Eqn. C1). "Number" is a key for the method in Table C2.

Number	Source	β	k	Note
1	Guzzetti et al. (2009)	1.450	0.074	worldwide study
2	Jaboyedoff et al. (2020)	1.362	0.288	similar to (1) without shallow or submarine landslides
3	Jaboyedoff et al. (2020)	1.375	0.410	mean of range for large landslides

Table C2. Geological characteristics of each site. "$V_{ls,X}$" are the estimated volumes of the instability, where X is either E for the volume determined using expert opinion, 1-3 using the empirical methods from Table C1, or S referring to the average of the volumes given by Schaefer et al. (2024). For Tyndall, the value in parentheses is the volume remaining at present-day. "A_{ls}" is the area of the instability from the delineated outline.

	Ellsworth	Portage	Barry	Yale	Columbia	Tyndall	Alsek	Grand Plateau
$\mathbf{V}_{ls,E}$ **[Mm^3]**	150	35	500	750	150	160 (100)	50	150
$\mathbf{V}_{ls,1}$ **[Mm^3]**	66	11	188	255	44	62	19	50
$\mathbf{V}_{ls,2}$ **[Mm^3]**	74	14	196	262	50	69	23	57
$\mathbf{V}_{ls,3}$ **[Mm^3]**	127	24	339	454	86	118	39	98
$\mathbf{V}_{ls,S}$ **[Mm^3]**	14-113	5-19	117-564	145-1025	17-111	-	-	-
$\mathbf{A}_{ls}$ **[km^2]**	1.5	0.4	3.1	3.8	1.1	1.4	0.6	1.2

https://doi.org/10.5194/egusphere-2024-1086
Preprint. Discussion started: 30 May 2024

Appendix D: Monthly meteorological data

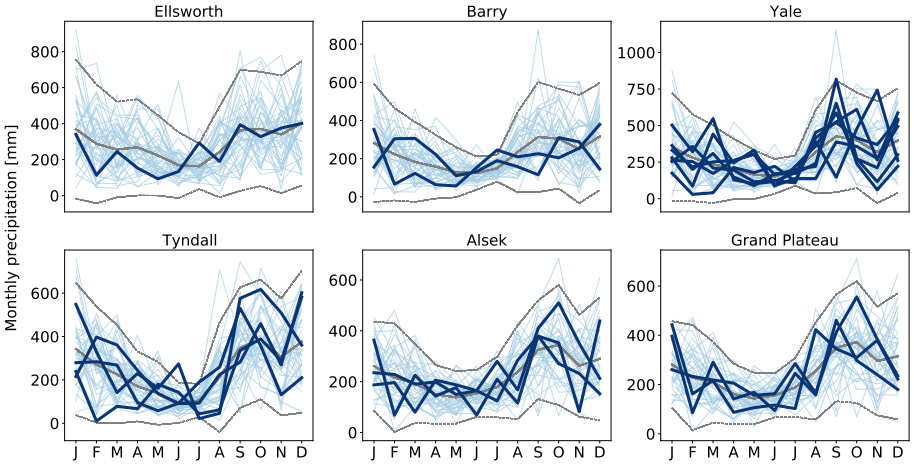

Figure D1. Average monthly precipitation at all sites which experienced a landslide acceleration during the study period. Thicker, darker blue lines correspond to the year or years during which the landslide accelerated, while light blue lines are all other years. The solid gray line corresponds to the mean monthly precipitation over the whole time period (1979-2022), and the gray dashed lines are two standard deviations above and below the mean. Note the differing y-axes of the various subplots. All x-axes refer to the labels on the bottom row.

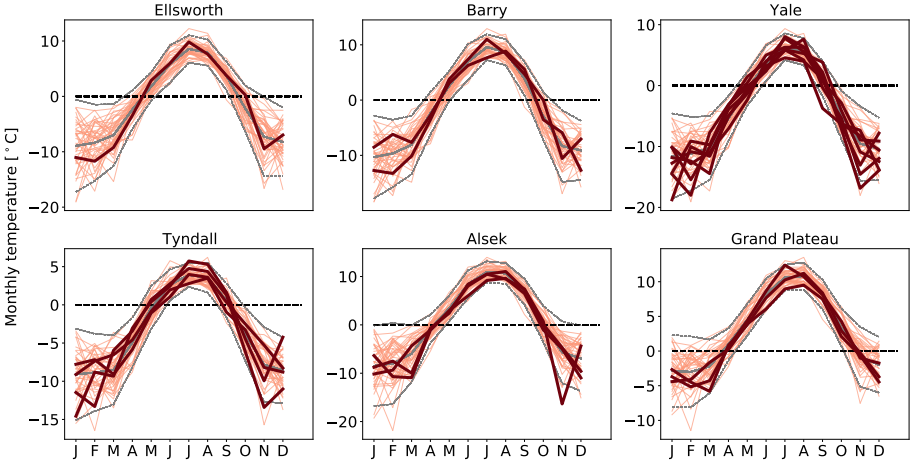

Figure D2. Average monthly temperature at all sites which experienced a landslide acceleration during the study period. Thicker, darker red lines correspond to the year or years during which the landslide accelerated, while light red lines are all other years. The solid gray line corresponds to the mean monthly temperature over the whole time period (1979-2022), and the gray dashed lines are two standard deviations above and below the mean. The black dashed line marks zero degrees Celsius. Note the differing y-axes of the various subplots. All x-axes refer to the labels on the bottom row.

https://doi.org/10.5194/egusphere-2024-1086
Preprint. Discussion started: 30 May 2024

Appendix E: Feature definition

Instability-adjacent-glacier polygon

We created an instability-adjacent-glacier polygon to examine the glacier changes near the instability. For sites where the instability is far from the current terminus, we created a glacier polygon that is the same width as the instability. For sites where the instability is currently near the terminus, we manually created a polygon around $1\,\mathrm{km}$ long starting from the smallest extent and then intersected this with the glacier outlines from RGI Consortium (2017). Note that the smallest extent of the glacier is not necessary at present-day.

Cross section

We generated cross sections through the landslide and glacier to study the glacier elevation changes near the instability. A line was drawn between the centroid of the instabilility polygon and the closest point on the centerline. Using the QGIS function "Extend lines," the line was extended by $4000\,\mathrm{m}$ in each direction. Points were then generated on the cross section at $10\,\mathrm{m}$ intervals using the QGIS function "Points along geometry." For these points, we then extracted values for each of the four available DEMs. For the cross section, we considered the area between the ridgetop behind the instability and the thickest part of the glacier.

https://doi.org/10.5194/egusphere-2024-1086
Preprint. Discussion started: 30 May 2024

Author contributions. MJ and BH conceptualized the study. JW completed the manual feature tracking analysis, mapped terminus locations, extracted ITS-LIVE velocities, and wrote the manuscript with the help of MJ and DF. BH provided landslide polygons and volumes, as well as helpful discussion about possible mechanisms. RH generated all co-registered DEMs. AM aided with the feature tracking and explanations of possible landslide mechanisms. DF supervised the overall work progress and helped in designing the figures. All co-authors read and provided feedback on the paper.

Competing interests. The authors declare that they have no conflict of interest.

Acknowledgements. We thank Maximillian Van Wyk de Vries and Amaury Dehecq for the helpful discussions about feature tracking, as well as Marit van Tiel for the useful input about glacier hydrology. We also thank Etienne Berthier and Amaury Dehecq for providing the 1960s and 1980s DEMs, respectively. Additionally, we thank Daniel Ben-Yehoshua for the interesting discussions about landslide-glacier interactions. BH acknowledges funding from the US National Science Foundation, award number 205210. RH acknowledges funding from the Swiss National Science Foundation, grant number 184634, as well as funding from NASA, award number 80NSSC22K1094.

https://doi.org/10.5194/egusphere-2024-1086
Preprint. Discussion started: 30 May 2024

References

Alaska Seismic Hazards Safety Commission: Report to the Governor and State Legislature, https://seismic.alaska.gov/download/ashsc_meetings_minutes/ASHSC_2012_annual_report.pdf, 2012.

Ballantyne, C. K.: Paraglacial geomorphology, Quaternary Science Reviews, p. 83, 2002.

Berthier, E., Schiefer, E., Clarke, G. K. C., Menounos, B., and Rémy, F.: Contribution of Alaskan Glaciers to Sea-Level Rise Derived from Satellite Imagery, Nature Geoscience, 3, 92–95, https://doi.org/10.1038/ngeo737, 2010.

Cody, E., Anderson, B. M., McColl, S. T., Fuller, I. C., and Purdie, H. L.: Paraglacial adjustment of sediment slopes during and immediately after glacial debuttressing, Geomorphology, 371, 107 411, https://doi.org/10.1016/j.geomorph.2020.107411, 2020.

Cuffey, K. M. and Paterson, W. S. B.: The Physics of Glaciers, Amsterdam Heidelberg: Butterworth-Heineman, 4 edn., 2010.

Dahl-Jensen, T., Larsen, L. M., Pedersen, S. A. S., Pedersen, J., Jepsen, H. F., Pedersen, G., Nielsen, T., Pedersen, A. K., Platen-Hallermund, F. V., and Weng., W.: Landslide and Tsunami 21 November 2000 in Paatuut, West Greenland, Natural Hazards, 31, 277–87, https://doi.org/10.1023/B:NHAZ.0000020264.70048.95, 2004.

Dai, C., Higman, B., Lynett, P. J., Jacquemart, M., Howat, I. M., Liljedahl, A. K., Dufresne, A., Freymueller, J. T., Geertsema, M., Ward Jones, M., and Haeussler, P. J.: Detection and Assessment of a Large and Potentially Tsunamigenic Periglacial Landslide in Barry Arm, Alaska, Geophysical Research Letters, 47, https://doi.org/10.1029/2020GL089800, 2020.

Dehecq, A., Gardner, A. S., nad Scott McMichael, O. A., Hugonnet, R., Shean, D., and Marty, M.: Automated Processing of Declassified KH-9 Hexagon Satellite Images for Global Elevation Change Analysis Since the 1970s, Frontiers in Earth Science, 8, https://www.frontiersin.org/articles/10.3389/feart.2020.566802, 2020.

Doi, I., Matsuura, S., Osawa, H., Shibasaki, T., and Tosa, S.: Effects of Coastal Erosion on Landslide Activity Revealed by Multi-sensor Observations, Earth Surface Processes and Landforms, 45, 2291–99, https://doi.org/10.1002/esp.4880, 2020.

Earthquake Hazards Program: 20 Largest Earthquakes in the World Since 1900, united States Geological Survey, https://www.usgs.gov/programs/earthquake-hazards/science/20-largest-earthquakes-world-1900, 2019.

Earthquake Hazards Program: Earthquake Magnitude, Energy Release, and Shaking Intensity, https://www.usgs.gov/programs/earthquake-hazards/earthquake-magnitude-energy-release-and-shaking-intensity, 2024.

Epprecht, W.: A Major Calving Event of Jakobshavns Isbræ, West Greenland, on 9 August 1982, Journal of Glaciology, 33, 169–172, doi:10.3189/S0022143000008650, 1987.

Fan, X., Dufresne, A., Subramanian, S. S., Strom, A., Hermanns, R., Stefanelli, C. T., Hewitt, K., Yunus, A. P., Dunning, S., Capra, L., Geertsema, M., Miller, B., Casagli, N., Jansen, J. D., and Xu, Q.: The Formation and Impact of Landslide Dams – State of the Art, Earth-Science Reviews, 203, https://doi.org/10.1016/j.earscirev.2020.103116, 2020.

Farinotti, D., Huss, M., Fürst, J. J., Landmann, J., Machguth, H., Maussion, F., and Pandit, A.: A consensus estimate for the ice thickness distribution of all glaciers on Earth, Nature Geoscience, 12, 168–173, https://doi.org/10.1038/s41561-019-0300-3, 2019.

Gardner, A. S., Moholdt, G., Scambos, T., Fahnstock, M., Ligtenberg, S., van den Broeke, M., and Nilsson, J.: Increased West Antarctic and unchanged East Antarctic ice discharge over the last 7 years, The Cryosphere, 12, 521–547, https://doi.org/10.5194/tc-12-521-2018, publisher: Copernicus GmbH, 2018.

Gardner, A. S., Fahnestock, M. A., and Scambos, T. A.: ITS_LIVE Regional Glacier and Ice Sheet Surface Velocities: Version 2, data archived at National Snow and Ice Data Center; https://doi:10.5067/6II6VW8LLWJ7., 2023.

https://doi.org/10.5194/egusphere-2024-1086
Preprint. Discussion started: 30 May 2024

Gischig, V., Preisig, G., and Eberhardt, E.: Numerical Investigation of Seismically Induced Rock Mass Fatigue as a Mechanism Contributing to the Progressive Failure of Deep-Seated Landslides, Rock Mechanics and Rock Engineering, 49, 2457–78, https://doi.org/10.1007/s00603-015-0821-z, 2016.

Glueer, F., Loew, S., Manconi, A., and Aaron, J.: From Toppling to Sliding: Progressive Evolution of the Moosfluh Landslide, Switzerland, Journal of Geophysical Research: Earth Surface, 124, 2899–2919, https://doi.org/10.1029/2019JF005019, 2019.

Glueer, F., Loew, S., and Manconi, A.: Paraglacial history and structure of the Moosfluh landslide (1850-2016), Switzerland, Geomorphology, 355, https://doi.org/10.1016/j.geomorph.2019.02.021, 2020.

Grämiger, L. M., Moore, J. R., Gischig, V. S., Ivy-Ochs, S., and Loew, S.: Beyond Debuttressing: Mechanics of Paraglacial Rock Slope Damage during Repeat Glacial Cycles: PARAGLACIAL ROCK SLOPE MECHANICS, Journal of Geophysical Research: Earth Surface, 122, 1004–36, https://doi.org/10.1002/2016JF003967, 2017.

Grämiger, L. M., Moore, J. R., Gischig, V. S., and Loew, S.: Thermomechanical Stresses Drive Damage of Alpine Valley Rock Walls During Repeat Glacial Cycles, Journal of Geophysical Research: Earth Surface, 123, 2620–46, https://doi.org/10.1029/2018JF004626, 2018.

Grämiger, L. M., Moore, J. R., Gischig, V. S., Loew, S., Funk, M., and Limpach, P.: Hydromechanical Rock Slope Damage During Late Pleistocene and Holocene Glacial Cycles in an Alpine Valley, Journal of Geophysical Research: Earth Surface, 125, https://doi.org/10.1029/2019JF005494, 2020.

Guzzetti, F., Ardizzone, F., Cardinali, M., Rossi, M., and Valigi, D.: Landslide volumes and landslide mobilization rates in Umbria, central Italy, Earth and Planetary Science Letters, 279, 222–229, https://doi.org/10.1016/j.epsl.2009.01.005, 2009.

Handwerger, A. L., Fielding, E. J., Huang, M., Bennett, G. L., Liang, C., and Schulz, W. H.: Widespread Initiation, Reactivation, and Acceleration of Landslides in the Northern California Coast Ranges Due to Extreme Rainfall, Journal of Geophysical Research: Earth Surface, 124, 1782–97, https://doi.org/10.1029/2019JF005035, 2019.

Handwerger, A. L., Fielding, E. J., Sangha, S. S., and Bekaert, D. P. S.: Landslide Sensitivity and Response to Precipitation Changes in Wet and Dry Climates, Geophysical Research Letters, 49, https://doi.org/10.1029/2022GL099499, 2022.

Hanson, B. and Hooke, R. L.: Glacier Calving: A Numerical Model of Forces in the Calving-Speed/Water-Depth Relation, Journal of Glaciology, 46, 188–96, https://doi.org/10.3189/172756500781832792, 2000.

Hermanns, R. L., Schleier, M., Böhme, M., Blikra, L. H., Gosse, J., Ivy-Ochs, S., and Hilger, P.: Rock-Avalanche Activity in W and S Norway Peaks After the Retreat of the Scandinavian Ice Sheet, in: Advancing Culture of Living with Landslides, edited by Mikoš, M., Vilímek, V., Yin, Y., and Sassa, K., pp. 331–38, Springer International Publishing, 2017.

Hersbach, H., Muñoz Sabater, J., Nicolas, Rozum, I., Simmons, Vamborg, F., Bell, B., Berrisford, P., Biavati, G., Buontempo, C., Horányi, A., Peubey, C., Radu, R., Schepers, D., Soci, C., Dee, D., and Thépaut, J.-N.: Essential climate variables for assessment of climate variability from 1979 to present, copernicus Climate Change Service (C3S) Data Store (CDS). (Accessed on 11-11-2022), 2018.

Higman, B.: Alaska inventory of landslides and slope instabilities, accessed April 12, 2022, 2022.

Higman, B., Shugar, D. H., Stark, C. P., Ekström, G., Koppes, M. N., Lynett, P., Dufresne, A., Haeussler, P. J., Geertsema, M., Gulick, S., Mattox, A., Venditti, J. G., Walton, M. A. L., McCall, N., Mckittrick, E., MacInnes, B., Bilderback, E. L., Tang, H., Willis, M. J., Richmond, B., Reece, R. S., Larsen, C., Olson, B., Capra, J., Ayca, A., Bloom, C., Williams, H., Bonno, D., Weiss, R., Keen, A., Skanavis, V., and Loso, M.: The 2015 landslide and tsunami in Taan Fiord, Alaska, Scientific Reports, 8, 12 993, https://doi.org/10.1038/s41598-018-30475-w, 2018.

Higman, B., Lahusen, S., Belair, G., Staley, D., and Jacquemart, M.: Inventory of Large Slope Instabilities, Prince William Sound, Alaska: U.S. Geological Survey data release, https://doi.org/10.5066/P9XGMHHP, 2023.

https://doi.org/10.5194/egusphere-2024-1086
Preprint. Discussion started: 30 May 2024

Hugonnet, R., McNabb, R., Berthier, E., Menounos, B., Nuth, C., Girod, L., Farinotti, D., Huss, M., Dussaillant, I., Brun, F., and Kääb, A.: Accelerated global glacier mass loss in the early twenty-first century, Nature, 592, 726–731, https://doi.org/10.1038/s41586-021-03436-z, 2021.

Hussain, M. and Mahmud, I.: pyMannKendall: a python package for non parametric Mann Kendall family of trend tests., Journal of Open Source Software, 4, 1556, https://doi.org/10.21105/joss.01556, 2019.

Immerzeel, W. W., Lutz, A. F., Andrade, M., Bahl, A., Biemans, H., Bolch, T., Hyde, S., Davies, B., Elmore, A. C., Emmer, A., Feng, M., Fernández, A., Haritashya, U., Kargel, J. S., Koppes, M., Kraaijenbrink, P. D. A., Kulkarni, A. V., Mayewski, P. A., Nepal, S., Pacheco, P., Painter, T. H., Pellicciotti, F., Rajaram, H., Rupper, S., Sinisalo, A., Shrestha, A. B., Viviroli, D., Wada, Y., Xiao, C., Yao, T., and Baillie, J. E. M.: Importance and Vulnerability of the World's Water Towers, Nature, 577, 364–69, https://doi.org/10.1038/s41586-019-1822-y, 2020.

IPCC: Summary for Policymakers, in: IPCC Special Report on the Ocean and Cryosphere in a Changing Climate, edited by Pörtner, H. O., Roberts, D., Masson-Delmotte, V., Zhai, V., Tignor, M., Poloczanska, E., Mintenbeck, K., Alegría, A., Nicolai, M., Okem, A., Petzold, J., Rama, B., and Weyer, N., pp. 3–35, Cambridge University Press, Cambridge, UK and New York, NY, USA, https://doi.org/10.1017/9781009157964.001, 2019.

IPCC: in: Climate Change 2022: Impacts, Adaptation, and Vulnerability. Contribution of Working Group II to the Sixth Assessment Report of the Intergovernmental Panel on Climate Change, edited by Pörtner, H. O., Roberts, D., Tignor, M., Poloczanska, E., Mintenbeck, K., Alegría, A., Craig, M., Langsdorf, S., Löschke, S., Möller, V., Okem, A., and Rama, B., p. 3056, Cambridge University Press, Cambridge, UK and New York, NY, USA, doi:10.1017/9781009325844, 2022.

Iverson, R. M.: Landslide Triggering by Rain Infiltration, Water Resources Research, 36, 1897–1910, https://doi.org/10.1029/2000WR900090, 2000.

Jaboyedoff, M., Carrea, D., Derron, M.-H., Oppikofer, T., Penna, I. M., and Rudaz, B.: A Review of Methods Used to Estimate Initial Landslide Failure Surface Depths and Volumes, Engineering Geology, 267, https://doi.org/10.1016/j.enggeo.2020.105478, 2020.

Kanamori, H.: The Energy Release in Great Earthquakes, Journal of Geophysical Research, 82, 2981–87, https://doi.org/10.1029/JB082i020p02981, 1977.

Keefer, D. K.: Landslides caused by earthquakes, GSA Bulletin, 4, 406–421, 1984.

Kim, J., Coe, J. A., Lu, Z., Avdievitch, N. N., and Hults, C. P.: Spaceborne InSAR Mapping of Landslides and Subsidence in Rapidly Deglaciating Terrain, Glacier Bay National Park and Preserve and Vicinity, Alaska and British Columbia, Remote Sensing of Environment, 281, 113 231, https://doi.org/10.1016/j.rse.2022.113231, 2022.

Kos, A., Amann, F., Strozzi, T., Delaloye, R., Ruette, J., and Springman, S.: Contemporary glacier retreat triggers a rapid landslide response, Great Aletsch Glacier, Switzerland, Geophysical Research Letters, 43, https://doi.org/10.1002/2016GL071708, 2016.

Lacroix, P., Handwerger, A. L., and Bièvre, G.: Life and Death of Slow-Moving Landslides, Nature Reviews Earth & Environment, 1, 404–19, https://doi.org/10.1038/s43017-020-0072-8, 2020.

Lacroix, P., Belart, J. M. C., Berthier, E., Sæmundsson, P., and Jónsdóttir, K.: Mechanisms of Landslide Destabilization Induced by Glacier-Retreat on Tungnakvíslarjökull Area, Iceland, Geophysical Research Letters, 49, https://doi.org/10.1029/2022GL098302, 2022.

Larsen, C., Motyka, R., Freymueller, J., Echelmeyer, K., and Ivins, E.: Rapid Viscoelastic Uplift in Southeast Alaska Caused by Post-Little Ice Age Glacial Retreat, Earth and Planetary Science Letters, 237, 548–60, https://doi.org/10.1016/j.epsl.2005.06.032, 2005.

Lemaire, E., Dufresne, A., Hamdi, P., Higman, B., Wolken, G. J., and Amann, F.: Back-Analysis of the Paraglacial Slope Failure at Grewingk Glacier and Lake, Alaska, Landslides, https://doi.org/10.1007/s10346-023-02177-6, 2023a.

https://doi.org/10.5194/egusphere-2024-1086
Preprint. Discussion started: 30 May 2024

Lemaire, E., Dufresne, A., Hamdi, P., Higman, B., Jacquemart, M., Walden, J., and Amann, F.: Analysis of the unstable slope above Portage Glacier (Alaska) through conventional and remote sensing approaches, 6th World Landslide Forum, Florence, Italy, THEME 2: REMOTE SENSING, MONITORING AND EARLY WARNING, 2023b.

Loso, M. G., Larsen, C. F., Tober, B. S., Christoffersen, M., Fahnestock, M., Holt, J. W., and Truffer, M.: Quo Vadis, Alsek? Climate-Driven Glacier Retreat May Change the Course of a Major River Outlet in Southern Alaska, Geomorphology, 384, 107 701, https://doi.org/10.1016/j.geomorph.2021.107701, 2021.

Manconi, A.: How Phase Aliasing Limits Systematic Space-Borne DInSAR Monitoring and Failure Forecast of Alpine Landslides, Engineering Geology, 287, 106 094, https://doi.org/10.1016/j.enggeo.2021.106094, 2021.

McColl, S. T.: Landslide Causes and Triggers, in: Landslide Hazards, Risks, and Disasters, pp. 17–42, Elsevier, https://doi.org/10.1016/B978-0-12-396452-6.00002-1, 2015.

McColl, S. T. and Davies, T. R. H.: Large ice-contact slope movements: glacial buttressing, deformation and erosion: Slope movement; glaicer deformation; erosion and entrainment, Earth Surface Processes and Landforms, 38, 1102–1115, https://doi.org/10.1002/esp.3346, 2013.

McNabb, R. W., Hock, R., and Huss, M.: Variations in Alaska tidewater glacier frontal ablation, 1985–2013, Journal of Geophysical Research: Earth Surface, 120, 120–136, https://doi.org/10.1002/2014JF003276, 2015.

Millan, R., Mouginot, J., Rabatel, A., and Morlighem, M.: Ice velocity and thickness of the world's glaciers, Nature Geoscience, 15, 124–129, https://doi.org/10.1038/s41561-021-00885-z, number: 2 Publisher: Nature Publishing Group, 2022.

Miller, D. J.: The Alaska earthquake of July 10, 1958: Giant wave in Lituya Bay, Bulletin of the Seismological Society of America, 50, 253–266, https://doi.org/10.1785/BSSA0500020253, 1960.

Mériaux, A., Sieh, K., Finkel, R. C., Rubin, C. M., Taylor, M. H., Meltzner, A. J., and Ryerson, F. J.: Kinematic Behavior of Southern Alaska Constrained by Westward Decreasing Postglacial Slip Rates on the Denali Fault, Alaska, Journal of Geophysical Research: Solid Earth, 114, https://doi.org/10.1029/2007JB005053, 2009.

Nuth, C. and Kääb, A.: Co-Registration and Bias Corrections of Satellite Elevation Data Sets for Quantifying Glacier Thickness Change, The Cryosphere, 5, 271–90, https://doi.org/10.5194/tc-5-271-2011, 2011.

Obu, J., Westermann, S., Kääb, A., and Bartsch, A.: Ground Temperature Map, 2000-2016, Northern Hemisphere Permafrost, alfred Wegener Institute, Helmholtz Centre for Polar and Marine Research, Bremerhaven, PANGAEA, https://doi.org/10.1594/PANGAEA.888600, 2018.

Okal, E. A.: Seismic Parameters Controlling Far-Field Tsunami Amplitudes: A Review, Natural Hazards, 1, 67–96, https://doi.org/10.1007/BF00168222, 1988.

Payo, A., Hall, J. W., French, J., Sutherland, J., Maanen, B. V., Nicholls, R. J., and Reeve, D. E.: Causal Loop Analysis of Coastal Geomorphological Systems, Geomorphology, 256, 36–48, https://doi.org/10.1016/j.geomorph.2015.07.048, 2016.

Porter, C., Morin, P., Howat, I., Noh, M.-J., Bates, B., Peterman, K., Keesey, S., Schlenk, M., Gardiner, J., Tomko, K., Willis, M., Kelleher, C., Cloutier, M., Husby, E., Foga, S., Nakamura, H., Platson, M., Wethington, Michael, J., Williamson, C., Bauer, G., Enos, J., Arnold, G., Kramer, W., Becker, P., Doshi, A., D'Souza, C., Cummens, P., Laurier, F., and Bojesen, M.: ArcticDEM, Version 3, https://doi.org/10.7910/DVN/OHHUKH, 2018.

Ravier, E. and Buoncristiani, J.-F.: Glaciohydrogeology, in: Past Glacial Environments, pp. 431–66, Elsevier, https://doi.org/10.1016/B978-0-08-100524-8.00013-0, 2018.

RGI Consortium: Randolph Glacier Inventory - A Dataset of Global Glacier Outlines, Version 6, boulder, Colorado USA. NSIDC: National Snow and Ice Data Center. doi: https://doi.org/10.7265/4m1f-gd79, 2017.

https://doi.org/10.5194/egusphere-2024-1086
Preprint. Discussion started: 30 May 2024

Rounce, D. R., Hock, R., Maussion, F., Hugonnet, R., Kochtitzky, W., Huss, M., Berthier, E., Brinkerhoff, D., Compagno, L., Copland, L., Farinotti, D., Menounos, B., and McNabb, R. W.: Global Glacier Change in the 21st Century: Every Increase in Temperature Matters, Science, 379, 78–83, https://doi.org/10.1126/science.abo1324, 2023.

Schaefer, L., Coe, J. A., Jones, K. W., Collins, B. D., Staley, D. M., West, M., Karasozen, E., Miles, C., Wolken, G., Daanen, R., and Baxstrom, K.: Kinematic Evolution of a Large Paraglacial Landslide in the Barry Arm Fjord of Alaska, Journal of Geophysical Research: Earth Surface, 128, https://doi.org/10.1029/2023JF007119, 2023.

Schaefer, L., Kim, J., Staley, D., Lu, Z., and Barnhart, K.: Satellite interferometry landslide detection and preliminary tsunamigenic plausibility assessment in Prince William Sound, southcentral Alaska, Tech. rep., U.S. Geological Survey Open-File Report 2023–1099, https://doi.org/10.3133/ofr20231099, 2024.

Sharma, S., Talchabhadel, R., Nepal, S., Ghimire, G. R., Rakhal, B., Panthi, J., Adhikari, B. R., Pradhanang, S. M., Maskey, S., and Kumar, S.: Increasing Risk of Cascading Hazards in the Central Himalayas, Natural Hazards, 119, 1117–26, https://doi.org/10.1007/s11069-022-05462-0, 2023.

Shugar, D.H. et al.: A massive rock and ice avalanche caused the 2021 disaster at Chamoli, Indian Himalaya, Science, 373, 300–306, dOI:10.1126/science.abh4455, 2021.

Shulski, M. and Wendler, G.: The Climate of Alaska, University of Alaska Press, https://books.google.ch/books?id=aUDWK8zDr50C, 2007.

Song, C., Yu, C., Li, Z., Utili, S., Frattini, P., Crosta, G., and Peng, J.: Triggering and Recovery of Earthquake Accelerated Landslides in Central Italy Revealed by Satellite Radar Observations, Nature Communications, 13, 7278, https://doi.org/10.1038/s41467-022-35035-5, 2022.

Storni, E., Hugentobler, M., Manconi, A., and Loew, S.: Monitoring and analysis of active rockslide-glacier interactions (Moosfluh, Switzerland), Geomorphology, 371, 107 414, https://doi.org/10.1016/j.geomorph.2020.107414, 2020.

Strzelecki, M. C. and Jaskólski, M. W.: Arctic tsunamis threaten coastal landscapes and communities – survey of Karrat Isfjord 2017 tsunami effects in Nuugaatsiaq, western Greenland, Natural Hazards Earth System Science, 20, 2521–2534, https://doi.org/10.5194/nhess-20-2521-2020, 2020.

U.S. Geological Survey: Earthquakes, https://earthquake.usgs.gov/earthquakes/map/, 2023.

U.S. Geological Survey and Alaska Department of Natural Resources: Quaternary Fault and Fold Database of the United States, https://www.usgs.gov/programs/earthquake-hazards/faults, 2024.

Van Wyk de Vries, M., Wickert, A. D., MacGregor, K. R., Rada, C., and Willis, M. J.: Atypical landslide induces speedup, advance, and long-term slowdown of a tidewater glacier, Geology, https://doi.org/10.1130/G49854.1, 2022.

Weertman, J.: Stability of the Junction of an Ice Sheet and an Ice Shelf, Journal of Glaciology, 13, 3–11, https://doi.org/10.3189/S0022143000023327, 1974.

Wiles, G. C. and Calkin, P. E.: Reconstruction of a Debris-Slide-Initiated Flood in the Southern Kenai Mountains, Alaska, Geomorphology, 5, 535–46, https://doi.org/10.1016/0169-555X(92)90024-I, 1992.

Wilson, F., Hults, C., Mull, C., and Karl, S.: Geologic map of Alaska: U.S. Geological Survey Scientific Investigations Map SIM-3340, https://doi.org/10.3133/sim3340, 2015.

Windnagel, A., Hock, R., Maussion, F., Paul, F., Rastner, P., Raup, B., and Zemp, M.: Which glaciers are the largest in the world?, Journal of Glaciology, 69, 301–310, doi:10.1017/jog.2022.61, 2023.

xdem contributors: Xdem, Zenodo [code], https://doi.org/10.5281/zenodo.4809697, 2021.